Product Traceability and Uncertainty for the temperature profile lidar product

Version 0.4

GAIA-CLIM
Gap Analysis for Integrated
Atmospheric ECV Climate Monitoring
Mar 2015 - Feb 2018

A Horizon 2020 project; Grant agreement: 640276

Date: 19 January 2018

Dissemination level: Final

Work Package 2; Compiled by
Arnoud Apituley, Anne van Gijsel (KNMI)

Royal Netherlands
Meteorological Institute
Ministry of Infrastructure
and Water Management

Table of Contents

Version history

Version	Principal updates	Owner	Date
0.3 draft	First draft	KNMI	12.12.2017
0.4 draft	Advanced draft	KNMI	11.01.2018
0.4e	Incorporating TG's comments	KNMI	15.01.2018
0.4f	Final draft	KNMI	16.01.2018
0.4g	Final version	KNMI	02.02.2018

1 Product overview

Product name: Temperature profile
Product technique: Rayleigh/Mie, Raman Lidar
Product measurand: Temperature (T)
Product form/range: profile (ground to 110 km, 15/30 to 70 km, 1-8 hours averaged)
Product dataset: Temperature profile
Site/Sites/Network location:

- Table Mountain, Wrightwood CA, USA
- Mauna Loa, Hawaii, USA
- Purple Crow Lidar, Ontario, Canada

Product time period: Jan 1 – Dec 31, 2014
Data provider: NDACC
Instrument provider: Various
Product assessor: Arnoud Apituley, KNMI
Assessor contact email: apituley@knmi.nl

1.1 Guidance notes

For general guidance see the Guide to Uncertainty in Measurement & its Nomenclature, published as part of the GAIA-CLIM project.

This document is a measurement product technical document which should be stand-alone i.e. intelligible in isolation. Reference to external sources (preferably peer-reviewed) and documentation from previous studies is clearly expected and welcomed, but with sufficient explanatory content in the GAIA CLIM document not to necessitate the reading of all these reference documents to gain a clear understanding of the GAIA CLIM product and associated uncertainties entered into the Virtual Observatory (VO).

In developing this guidance, we have created a convention for the traceability identifier numbering as shown in Figure 1. The 'main chain' from raw measurand to final product forms the axis of the diagram, with top level identifiers (i.e. 1, 2, 3 etc.). Side branch processes add sub-levels components to the top level identifier (for example, by adding alternate letters & numbers, or 1.3.2 style nomenclature).

The key purpose of this sub-level system is that all the uncertainty from a sub-level are summed in the next level up.

For instance, using Figure 1, contributors 2a1, 2a2 and 2a3 are all assessed as separate components to the overall traceability chain (have a contribution table). The contribution table for (and uncertainty associated with) 2a, should combine all the sub-level uncertainties (and any additional uncertainty intrinsic to step 2a). In turn, the contribution table for contributor 2, should include all uncertainties in its sub-levels.

Therefore, only the top level identifiers (1, 2, 3, etc.) shown in bold in the summary table need be combined to produce the overall product uncertainty. The branches can therefore be considered in isolation, for the more complex traceability chains, with the top level contribution table transferred to the main chain. For instance, see Figure 2 & Figure 3 as an example of how the chain can be divided into a number of diagrams for clearer representation.

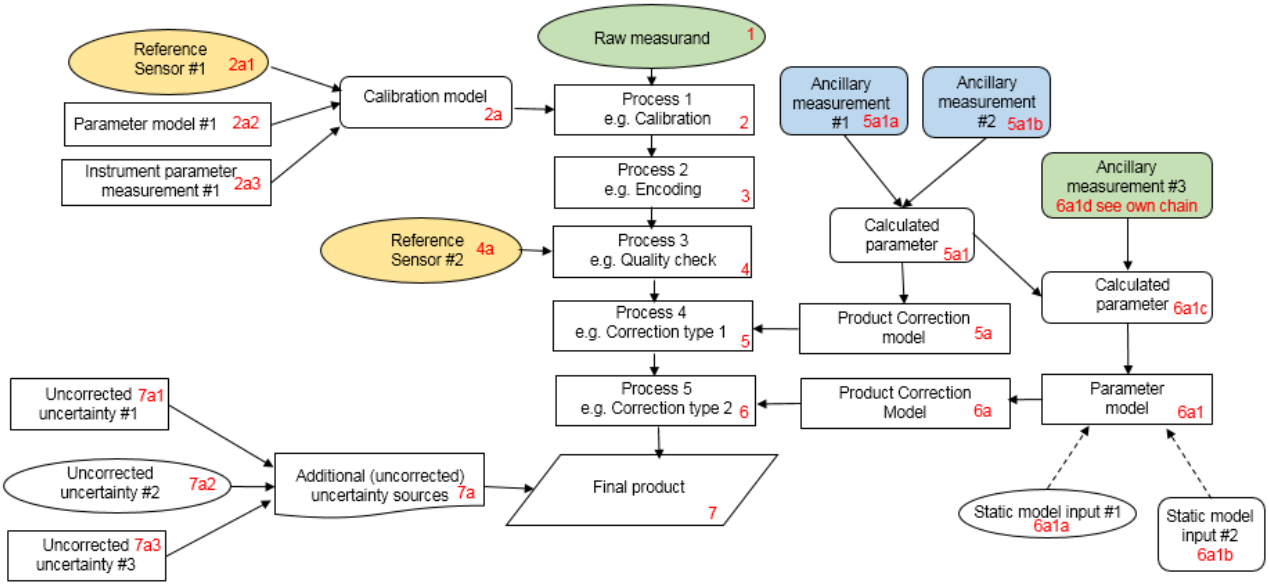

Figure 1. Example traceability chain. Green represents a key measurand or ancillary measurand recorded at the same time with the product raw measurand. Yellow represents a source of traceability. Blue represents a static ancillary measurement

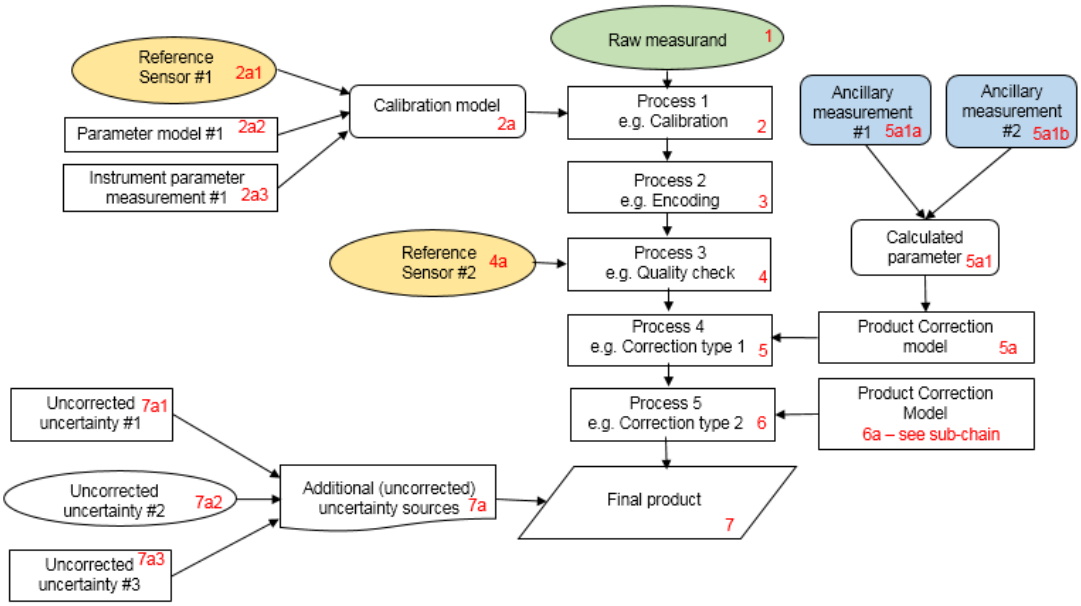

Figure 2. Example chain as sub-divided chain. Green represents a key measurand or ancillary measurand recorded at the same time with the product raw measurand. Yellow represents a source of traceability. Blue represents a static ancillary measurement

When deciding where to create an additional sub-level, the most appropriate points to combine the uncertainties of sub-contributions should be considered, with additional sub-levels used to illustrate where their contributions are currently combined in the described process.

A short note on colour coding. Colour coding can/should be used to aid understanding of the key contributors, but we are not suggesting a rigid framework at this time. In Figure 1, green represents a key measurand or ancillary or complementary measurand recorded at the same time with the raw measurand; yellow represents a primary source of traceability & blue represents a static ancillary measurement (site location, for instance). Any colour coding convention you use, should be clearly described.

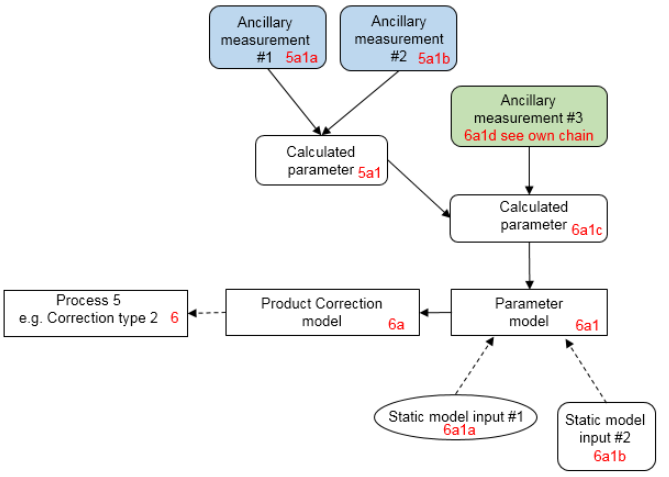

Figure 3. Example chain contribution 6a sub-chain. Green represents a key measurand or ancillary measurand recorded at the same time with the product raw measurand. Blue represents a static ancillary measurement

The contribution table to be filled for each traceability contributor has the form seen in Table 1.

Table 1. The contributor table.

Information / data	Type / value / equation	Notes / description
Name of effect		
Contribution identifier		
Measurement equation parameter(s) subject to effect		
Contribution subject to effect (final product or sub-tree intermediate product)		
Time correlation extent & form		
Other (non-time) correlation extent & form		
Uncertainty PDF shape		
Uncertainty & units		
Sensitivity coefficient		
Correlation(s) between affected parameters		
Element/step common for all sites/users?		
Traceable to …		
Validation		

Name of effect – The name of the contribution. Should be clear, unique and match the description in the traceability diagram.

Contribution identifier - Unique identifier to allow reference in the traceability chains.

Measurement equation parameter(s) subject to effect – The part of the measurement equation influenced by this contribution. Ideally, the equation into which the element contributes.

Contribution subject to effect – The top level measurement contribution affected by this contribution. This can be the main product (if on the main chain), or potentially the root of a side branch contribution. It will depend on how the chain has been sub-divided.

Time correlation extent & form – The form & extent of any correlation this contribution has in time.

Other (non-time) correlation extent & form – The form & extent of any correlation this contribution has in a non-time domain. For example, spatial or spectral.

Uncertainty PDF shape – The probability distribution shape of the contribution, Gaussian/Normal Rectangular, U-shaped, log-normal or other. If the form is not known, a written description is sufficient.

Uncertainty & units – The uncertainty value, including units and confidence interval. This can be a simple equation, but should contain typical values.

Sensitivity coefficient – Coefficient multiplied by the uncertainty when applied to the measurement equation.

Correlation(s) between affected parameters – Any correlation between the parameters affected by this specific contribution. If this element links to the main chain by multiple paths within the traceability chain, it should be described here. For instance, SZA or surface pressure may be used separately in a number of models & correction terms that are applied to the product at different points in the processing. See Figure 1, contribution 5a1, for an example.

Element/step common for all sites/users – Is there any site-to-site/user-to-user variation in the application of this contribution?

Traceable to – Describe any traceability back towards a primary/community reference.

Validation – Any validation activities that have been performed for this element?

2 Introduction

This document presents the Product Traceabililty and Uncertainty (PTU) information for temperature profiles retrieved with Rayleigh/Mie and Raman lidars. It does not cover measurements made with the pure rotational Raman, DIAL, Brillouin-Doppler nor optimal estimation techniques, and not for resonance fluorescence lidar observations. Specifically, we will focus on discussing the uncertainties associated with the temperature retrieval using the density integration technique. The aim of this document is to provide supporting information for the users of this product within the GAIA-CLIM VO. The uncertainty and traceability information contained in this document is based on the details given in Leblanc et al. (2016c, 2016d).

Leblanc et al. (2016c) describe an approach for the definition, propagation, and reporting of uncertainty in the temparture profile lidar data products contributing to the Network for the Detection for Atmospheric Composition Change (NDACC) database. One essential aspect of the proposed approach is the propagation in parallel of all independent uncertainty components through the data

processing chain before they are combined together to form the temperature combined standard uncertainty.

The independent uncertainty components contributing to the overall budget cover signal detection, saturation correction, background noise extraction, and temperature to tie-on at the top of the profile, as well as minor components such as absorption cross-sections of ozone and NO_2, the molecular extinction cross-sections, the use of ancillary air, ozone, and NO_2 number densities, the acceleration of gravity, and the molecular mass of air. The expression of the individual uncertainty components and their step-by-step propagation through the temperature profile processing chain are thoroughly estimated. All sources of uncertainty except detection noise imply correlated terms in the vertical dimension, which requires knowledge of the covariance matrix when the lidar signal is integrated from the top of the profile.

The temperature uncertainty budget is presented as much as possible in a generic form (i.e., as a function of instrument performance and wavelength) so that investigators can calculate uncertainty estimates for their own instrument in a straightforward manner and assess the expected impact. The approach and recommendations described here apply to the density integration technique (Hauchecorne and Chanin, 1980), but not to the Optimal Estimation Method (OEM; Sica and Haefele, 2015), for which vertical resolution and uncertainties are computed implicitly by the OEM.

3 Instrument description

The basic setup of a typical, vertically pointing lidar system is shown in Figure 4. The lidar technique, acronym for "light detection and ranging", is based on the transmission into the atmosphere of short light pulses, with duration ranging from a few to several hundreds of nanoseconds, by a laser transmitter, directly or by means of transmission optics. In any point of the atmospheric volume crossed by the laser beam, a portion of the incident light is backscattered by atmospheric constituents. This backscattered light is collected by a receiving telescope. The light received from the atmosphere passes through an optical system, consisting of various elements (lenses, mirrors, filters, etc.), which selects specific wavelengths of the light collected by the telescope. The light from the optical system is forwarded to detectors, typically photomultipliers that convert the light into electrical signals.

An electronic trigger circuit synchronizes the data acquisition to start with the emission of each laser pulse so that atmospheric signals are acquired as a function of elapsed time with respect to the emission of each laser pulse, from which distance can be inferred unambiguously. These signals are the lidar signals, measuring the intensity of the light backscattered by the atmosphere as a function of the distance from the lidar.

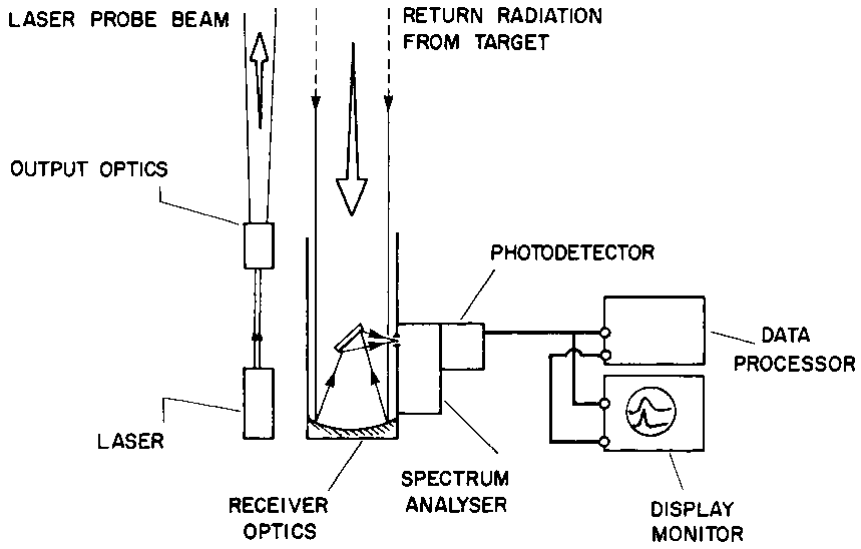

Figure 4. Schematic of a basic vertically pointing lidar system (Measures, 1984)

Temperature profiles in the middle atmosphere (15-80 km) have been measured by lidar since the 1980s using the density integration technique (e.g., Hauchecorne and Chanin, 1980; Keckhut et al., 1993, 2011). In the articles describing these measurements, the uncertainty is often limited to statistical noise (e.g., Hauchecorne and Chanin, 1980), and it is less common to include other components such as saturation (e.g., Leblanc et al., 1998), ozone absorption correction (Sica et al., 2001) or the initialization of temperature with an external data source at the top of the profile (Argall, 2007). Leblanc et al. (1998) provide a review of the most common error sources made in the lidar temperature retrievals which were assessed with synthetic lidar signals. NDACC intercomparison campaigns have also contributed to assessing lidar measurement uncertainties (Keckhut et al., 2004).

3.1 Retrieval methodology

To retrieve a temperature profile in the stratosphere or mesosphere using the density integration technique, we start from the Lidar Equation (e.g., Hinkley, 1976; Weitkamp, 2005). This equation in its most compressed form describes the emission of light by a laser source, its backscatter at altitude z, its extinction and scattering along its path up and back, and its collection back on a detector:

$$P(z,\lambda_E,\lambda_R) = P_L(\lambda_E)\frac{\eta(z,\lambda_R)\delta z}{(z-z_L)^2}\tau_{UP}(z,\lambda_E)\beta(z,\lambda_E,\lambda_R)\tau_{DOWN}(z,\lambda_R) \quad (1)$$

– λ_E is the laser emission wavelength and λ_R is the receiver detection wavelength;
– P is the total number of photons collected at wavelength λ_R on the lidar detector surface;
– δz is the thickness of the backscattering layer sounded during the time interval δt ($\delta z = c\delta t/2$, where c is the speed of light);
– P_L is the number of photons emitted at the emission wavelength λ_E;
– η is the optical efficiency of the receiving channel, including optical and spectral transmittance and geometric obstruction;
– z is the altitude of the backscattering layer;
– z_L is the altitude of the lidar (laser and receiver assumed to be at the same altitude);
– β is the total backscatter coefficient (including particulate β_P and molecular β_M backscatter);
– τ_{UP} is the optical thickness integrated along the outgoing beam path between the lidar and the scattering altitude z, and is defined as

$$\tau_{UP}(z) = \exp\left[-\int_{z_L}^{z} \left(\sigma_M(\lambda_E) N_a(z') + \alpha_P(z', \lambda_E) + \sum_i \sigma_i(z', \lambda_E) N_i(z') \right) dz' \right] \quad (2)$$

– τ_{DOWN} is the optical thickness integrated along the returning beam path between the scattering altitude z and the lidar receiver, and is defined as

$$\tau_{DOWN}(z) = \exp\left[-\int_{z_L}^{z} \left(\sigma_M(\lambda_R) N_a(z') + \alpha_P(z', \lambda_R) + \sum_i \sigma_i(z', \lambda_R) N_i(z') \right) dz' \right] \quad (3)$$

where σ_M is the molecular extinction cross section due to Rayleigh scattering (Strutt, 1899) (hereafter called "Rayleigh cross section" for brevity), N_a is the air number density, α_P is the particulate extinction coefficient, σ_i is the absorption cross section of absorbing constituent i, and N_i is the number density of absorbing constituent i. For altitudes between the ground and 90 km, the Rayleigh cross-sections can be considered constant with altitude, and therefore depend only on wavelength. The absorption cross-sections however are in most cases temperature-dependent, and should be taken as a function of both altitude and wavelength. Temperature is retrieved by inverting Eq. (1) with respect to the backscatter term β.

If there are no aerosols present, the backscatter coefficient β and, thus, the lidar signal collected on the detector are proportional to the air number density. Temperature can then be computed by vertically integrating the air number density under the assumptions that there is a hydrostatic balance and that the air is an ideal gas (Hauchecorne and Chanin, 1980). This inversion technique works for both elastic scattering (Rayleigh backscatter by the air molecules) and inelastic scattering (vibrational Raman backscatter by the nitrogen molecules) (Strauch et al., 1971; Gross et al., 1997). The backscatter coefficient can generically be written as a function of air number density N_a:

$$\beta(z) = \sigma_\beta N_a(z) \quad (4)$$

For Rayleigh backscatter, the effective cross-section σ_β is the molecular (Rayleigh) scattering cross-section at the emission wavelength λ_E:

$$\sigma_\beta = \sigma_M(\lambda_E) \quad (5)$$

For Raman backscatter, the effective cross-section σ_β is the vibrational Raman scattering cross-section of a well-mixed gas (typically nitrogen) at the Raman-shifted wavelength λ_R, multiplied by the mixing ratio of the well-mixed gas (e.g., 0.781 for nitrogen):

$$\sigma_\beta = 0.781 \sigma_{N2}(\lambda_E, \lambda_R) \quad (6)$$

Substituting into the lidar equation Eq. (1), we obtain an expression of air number density as a function of the backscatter lidar signal:

$$N_a(z) = \frac{P(z, \lambda_E, \lambda_R)(z - z_L)^2}{\sigma_\beta \eta(z, \lambda_E, \lambda_R) \delta z P_L(\lambda_E) \tau_{UP}(z, \lambda_E) \tau_{DOWN}(z, \lambda_R)} \quad (7)$$

A temperature profile is then calculated assuming hydrostatic balance and assuming that the air is an ideal gas with a constant mean molecular mass:

$$T(z - \delta z) = \frac{N_a(z)}{N_a(z - \delta z)} T(z) + \frac{M_a}{R_a N_a(z - \delta z)} \overline{N_a}(z) \overline{g}(z) \delta z \quad (8)$$

T is the retrieved temperature, M_a is the molecular mass of dry air, Ra is the ideal gas constant, and g is the acceleration of gravity. The horizontal bar above N_a and g represents the average value of Na and g between z and z-δz. An essential aspect of the method is that all altitude-independent terms (e.g., Rayleigh cross-section, lidar receiver efficiency) cancel out when computing the ratio of air number density at altitudes z and z-δz.

In this PTU, we will not treat uncertainties originating from aerosols (particulate extinction and particulate backscatter), or clouds (causing multiple scattering), as these factors are usually avoided by taking observations in clear air. For instance, temperature profiles from Rayleigh channels start above 25 to 30 km, where air can be considered free from aerosols - unless there is a very large volcanic eruption inserting a substantial number of particles high into the stratosphere which has not been the case for many years. When present, the contribution of particulate extinction and backscatter and multiple scattering is highly variable and it is not feasible to propose a standardised treatment here, but we refer to the work done by Earlinet (Mattis et al., 2016). As most temperature profiles are reported starting at higher altitudes, uncertainty due to correcting for incomplete beam-telescope overlap (which applies only at altitudes in the lower free troposphere) is not treated here either.

To transform the theoretical to a real temperature measurement model, we will consider the following conditions.

1. For each lidar receiver channel, the actual raw signal R recorded in the data files is represented by a vector of discretized values rather than a continuous function of altitude range: $z \rightarrow z(k)$ and $R(z) \rightarrow R(k)$ for $k = 1, nk$.
2. Only channels operating in photon-counting mode are considered in this measurement model. The estimation of the uncertainty due to analog-to-digital signal conversion is highly instrument-dependent, and therefore no meaningful standardized recommendations can be made.
3. Only channels operating in photon-counting mode are considered hereafter. For analog channels, uncertainty due to analog-to-digital signal conversion needs to be estimated. This estimation is highly instrument-dependent, and no meaningful standardized recommendations can therefore be provided.
4. In photon-counting detection mode, the recorded signals result from nonlinear transfer of the detected signals due to the inability of the counting electronics to temporally discriminate a very large number of photon-counts reaching the detector ("pulse pile-up" effect resulting in signal saturation) (e.g., Müller, 1973; Donovan et al., 1993). In the present work, we consider the most frequent case of non-paralyzable photon-counting systems (i.e., using "non-extended dead time", Müller, 1973), which allows for an analytical correction of the pulse pile-up effect.

Given the above four condtions, the photon counts P reaching the detector of a given channel can be expressed as a function of the discretized raw signal R recorded in the data files at altitude z(k):

$$P(k) = \frac{R(k)}{1 - \tau \frac{c}{2\delta z L} R(k)} - B(k) \tag{9}$$

B is the sum of sky and electronic background noise, τ is the photon-counting hardware dead-time characterizing the pulse pile-up effect (sometimes called resolving time), c the speed of light, and L the number of laser pulses for which the signal was actually recorded in the data files.

5. The signal is then corrected for all known altitude-dependent factors according to Eq. (7). For a given channel operating at the emission wavelength λ_E and detection wavelength λ_R (λ_E and λ_R are identical for Rayleigh backscatter channels), N is then defined as the lidar-measured relative number density that can be written as a function of the saturation-background-corrected signal P:

$$N(k) = \frac{(z(k) - z_L)^2}{\eta(k)} P(k) \exp\left(\sum_{k'=0}^{k} \left(\left(\sigma_{M\_E} + \sigma_{M\_R}\right) N_a(k') + \sum_{ig} \left(\sigma_{ig\_E}(k') + \sigma_{ig\_R}(k')\right) N_{ig}(k') \right) \delta z \right) \tag{10}$$

Here, the efficiency factor η does not have to be known in an absolute manner, but only its variation with altitude range is of importance. Furthermore, if the observation can be considered to be with full overlap between the beam and the telescope field-of-view, η is constant with altitude and does not need to be included at all. The subscript "M" refers to the Rayleigh cross-sections and "ig" to the

absorption cross-sections of the interfering gases. The subscripts extensions *E* and *R* refer to the emitted (λ_E) and received wavelengths (λ_R) respectively.
With the assumption of full overlap, the lidar-measured relative number density differs from the air number density only by a constant multiplication factor, and therefore does not need to include any of the constant terms with altitude found in the lidar equation as these terms cancel out in the temperature integration process (which implies the ratio of density at two consecutive altitudes).

6. The temperature profile is initialised at the the top of the profile $z(k_{TOP})$ using an external temperature measurement $T_a(k_{TOP})$ in a procedure called the "temperature tie-on". Integrating the relative number density obtained from the lidar measurement, the temperature profile can be calculated downward. Eq. (8) then becomes:

$$T(k) = \frac{N(k_{TOP})}{N(k)} T_a(k_{TOP}) + \frac{M_a \delta z}{R_a N(k)} S(k) \tag{11}$$

where S(k) is the discretized version of the summation term in Eq. (7):

$$S(k) = \sum_{k'=k}^{kTOP-1} \overline{N}(k') \overline{g}(k') \tag{12}$$

The horizontal bar above *N* and *g* denotes the mean value of *N* and *g* in the vertical layer comprised between $z(k')$ and $z(k'+1)$. The lidar-derived relative density *N* can be approximated by an exponential function of altitude range, and the layer-averaged density is computed using its geometric mean:

$$\overline{N}(k') = \sqrt{N(k')N(k'+1)} \tag{13}$$

The Earth's gravity field is three-dimensional but its variation with longitude is so small that it can be approximated by a function of latitude and altitude only. For small vertical increments, the variation of *g* with height is nearly linear, and its layer-averaged value can be expressed as a function of the height h above the reference ellipsoid averaged between $z(k')$ and $z(k'+1)$:

$$\overline{g}(k') = g_0\left(1 + g_1 \overline{h}(k') + g_2 \overline{h}^2(k')\right) \tag{14}$$

The height above the reference ellipsoid averaged between $z(k')$ and $z(k'+1)$ takes the form:

$$\overline{h}(k') = \frac{1}{2}\left(h(k') + h(k'+1)\right) \tag{15}$$

The constants g_0, g_1 and g_2 in Eq. (14) relate to the Earth's geometry and to the geodetic latitude of the lidar site. The derivation of the constants g_0, g_1 and g_2 following the World Geodetic System (NIMA-WGS, 1984) is provided in Leblanc et al. (2016d, section 3.5).

7. Optional smoothing: As in any real physical measurement, detection noise induces undesired high-frequency noise in the raw lidar signals. This noise can be reduced by digitally filtering the signals and/or the retrieved temperature profiles. The filtering process impacts the propagation of uncertainties and therefore should be included in the measurement model. When filtering is applied to the lidar signal (i.e., before temperature is computed), the signal's exponential decrease with altitude must be taken into account. For a given altitude $z(k)$, the filtering process in this case therefore consists of convolving a set of filter coefficients c_p with the logarithm of the unsmoothed signal s_u ($s_u=R$ or $s_u=P$ or $s_u=N$) to obtain a smoothed signal s_m following:

$$s_m(k) = \exp\left(\sum_{p=-n}^{n} c_p(k) \log\left(s_u(k+p)\right)\right) \tag{16}$$

When vertical filtering is applied to the retrieved temperature profile, the filtering process at each individual altitude $z(k)$ consists of convolving the filter coefficients c_p with the unsmoothed temperature *T* to obtain a smoothed temperature T_m following the expression:

$$T_m(k) = \sum_{p=-n}^{n} c_p(k) T(k+p) \tag{17}$$

In Eqs. (16)-(17), the filter coefficients should be symmetric (c_p=c_{-p} for all p) to achieve proper smoothing. Their number and values determine which noise frequencies will be reduced most. A review of digital filtering and recommendations for the use of standardized vertical resolution definitions are provided in (Leblanc et al., 2016a).

8. Optional merging: Temperature lidar instruments are usually designed with multiple channels of varying signal intensity to maximize the overall altitude range of the profile. Here, the propagation of uncertainty is considered for two channels being merged to form a single profile. This profile covering the entire useful range of the instrument is typically obtained by combining the most accurate overlapping sections of the profiles retrieved from individual channels. Merging individual intensity channels into a single profile can be done either during lidar signal processing or after the temperature is calculated for each individual channel. The thickness of the transition region can vary from a few meters to a few kilometers, depending on the instrument and on the intensity of the channels considered.

When the merging procedure is applied before the temperature profile is computed, it can be done on the raw signals (s=R), the saturation-background corrected signals (s=P), or the lidar-derived relative density (s=N). The signals of the channels to combine are of different magnitude, and signal normalization of one channel with respect to the other is necessary before combining the channels (κ being the scaling factor). Since the signals decrease with altitude is nearly exponential, the merging procedure should be done on the logarithm of the signal rather than the signal itself. Considering a low-intensity channel i_L and a high-intensity channel i_H, and assuming that the transition region's bottom and top altitudes are $z(k_1)$ and $z(k_2)$ respectively, the merged signal s_M at any altitude bin k comprised between k_1 and k_2 is typically obtained by computing a weighted average of the log-signal values s_m (or s if unsmoothed) for each range and at the same altitude bin:

$$s_M(k) = \exp\left(w(k)\log(s(k,i_L)) + (1-w(k))\log(\kappa s(k,i_H))\right) \quad k_1 \le k \le k_2 \text{ and } 0 \le w(k) \le 1 \tag{18}$$

When the merging procedure is applied to the retrieved temperature profiles, the merged temperature T_M at any altitude bin k comprised between k_1 and k_2 is typically obtained by computing a weighted average of the temperature values T_m (or T if unsmoothed) retrieved for each range at the same altitude bin:

$$T_M(k) = w(k)T_m(k,i_L) + (1-w(k))T_m(k,i_H) \quad k_1 \le k \le k_2 \text{ and } 0 \le w(k) \le 1 \tag{19}$$

With this set of equations, the input quantities' standard uncertainty must be introduced, propagated through the temperature measurement model, and then combined to produce a temperature combined standard uncertainty profile.

The instrumentation-related input quantities to consider in the temperature uncertainty budget are:

1. Alignment
2. Detection noise inherent to photon-counting signal detection
3. Saturation (pulse pile-up) correction parameters (typically, photon-counters' dead-time τ)
4. Background noise extraction parameters (typically, fitting parameters for function B)

The last three will be grouped together as pre-processing steps.

Based on Eqs. (10)-(14), the additional input quantities to consider in the NDACC-lidar standardized temperature uncertainty budget are:

5. Rayleigh extinction cross-sections σ_M
6. Ancillary air number density profile Na (or temperature T_a and pressure p_a profiles)
7. Absorption cross-sections of the interfering gases σ_{ig}
8. Number density profiles N_{ig} (or mixing ratio profile q_{ig}) of the interfering species
9. Acceleration of gravity g
10. The molecular mass of air M_a

11. External (a priori) air temperature for tie-on at the top of the profile $T_a(k_{TOP})$

Besides these eleven factors, uncertainties due to vertical filtering of the lidar signal or the retrieved temperature profile will also be discussed next to the treatment of uncertainties originating from merging signals or retrieved temperature profiels from multiple channels.

The above input quantities are not listed in order of significance, but instead, in the order they are introduced into the lidar temperature model. Quantitatively, the most significant uncertainty components are typically detection noise (1) and temperature tie-on (10) at the top of the profile, and saturation correction (2) and molecular extinction (4 and 5) at the bottom of the profile. The interfering gases "*ig*" to consider in practice are ozone and NO_2. Because of either very low concentrations or very low values of their absorption cross-sections, no other atmospheric gases or molecules are known to interfere with the temperature retrieval. The impact of absorption by ozone on the temperature retrieval is very small (<0.1 K) if working at wavelengths near the ozone minimum absorption region (e.g., 355 nm, 387 nm), but can account for up to 1 K error if neglected when working in the Chappuis band (e.g., 532 nm and 607 nm). Conversely, absorption by NO_2 is very small for temperature retrievals in the Chappuis band, but can account for up to a 0.2 K error if neglected at 355 nm and 387 nm.

The uncertainty contribution of the acceleration of gravity is very small (<0.1 K) provided given an altitude-dependent formulation of gravity (e.g., Eq. (14)) (Lemoine et al., 1998). In the upper mesosphere, the change in the air major species' mixing ratio induces a change with altitude of the air molecular mass and Rayleigh scattering cross-sections. However the induced changes remain below 0.1 K below 90 km, which is much less than the expected uncertainty arising due to remaining sources such as detection noise and tie-on temperature uncertainty (Argall, 2007). For temperature profiles reaching 100 km or higher, the change of the molecular mass of air with altitude should be taken into account.

When the receiver field-of-view and the laser beam are known to not fully overlap, an additional "instrumentation-related" uncertainty component must be introduced to take into account the overlap correction (altitude-dependent term η in Eq. (10)). Also, if the lidar receiver uses very narrow filters (typically narrower than 0.7 nm), another "instrumentation-related" uncertainty component must be introduced to take this into account: the temperature dependence of the Raman backscatter cross-sections (causing again the term η in Eq. (10) to be altitude-dependent). Because the overlap function and the filter width and position are strongly instrument-dependent, a standardized approach for the treatment of those uncertainty components cannot be proposed here. In the rest of this work, we will therefore assume full overlap and wide-enough filters to prevent an altitude dependence of the lidar transmission function which is valid for the specific subset of lidars being characterised here. As stated above, and for consistency with the ozone and aerosol extinction PTUs, we will nevertheless briefly discuss alignment. The receiver optical parameters and the transmission system will not be treated as these factors are deemed to be of less importance for temperature retrievals.

The exact altitude of each data bin k can be determined experimentally, for example by tracking the exact position in the data stream of the laser beam backscattering off the laser room hatch (assuming that the receiver and the transmission of the laser beam in the atmosphere are located in the same room). The time (i.e., altitude) resolution of today's state-of-the-art lidar data acquisition hardware is very high (of the order of nanoseconds, i.e., a few meters). The exact altitude of the lidar instrument can also be determined to a precision better than a meter using the current standard geo-positioning methods. For well-designed and well-validated lidar instruments, there is therefore no uncertainty associated with the determination of altitude, and hence no uncertainty associated with the range correction (z^2) term in Eq. (10).

Uncertainties associated with fundamental physical constants will not be considered here, but we do

recommend to use the values reported by the International Council for Science (ICSU) Committee on Data for Science and Technology (CODATA, http://www.codata.org/), endorsed by the BIPM (Mohr et al., 2008). Note that if the uncertainty of a fundamental constant is of similar order of magnitude as that of some other uncertainty components already identified, then this constant must be included among the input quantities and its uncertainty should be taken into account and propagated just like all other input quantities.

4 Product Traceability Chain

The PTU is given below for temperature profile retrievals in the mesosphere, stratosphere and upper troposphere with lidar. The PTU is divided into two sections: the physical model is presented in Figure 5 and the processing model in Figure 6. The numbered boxes in these figures indicate the key elements in the PTU chain that are the main contributors to the overall measurement uncertainty. Each of these elements is discussed in Section 5. It is currently assumed that the contributions of the other (unnumbered) elements are negligible. There would be a clear benefit to evaluating these additional elements in future.

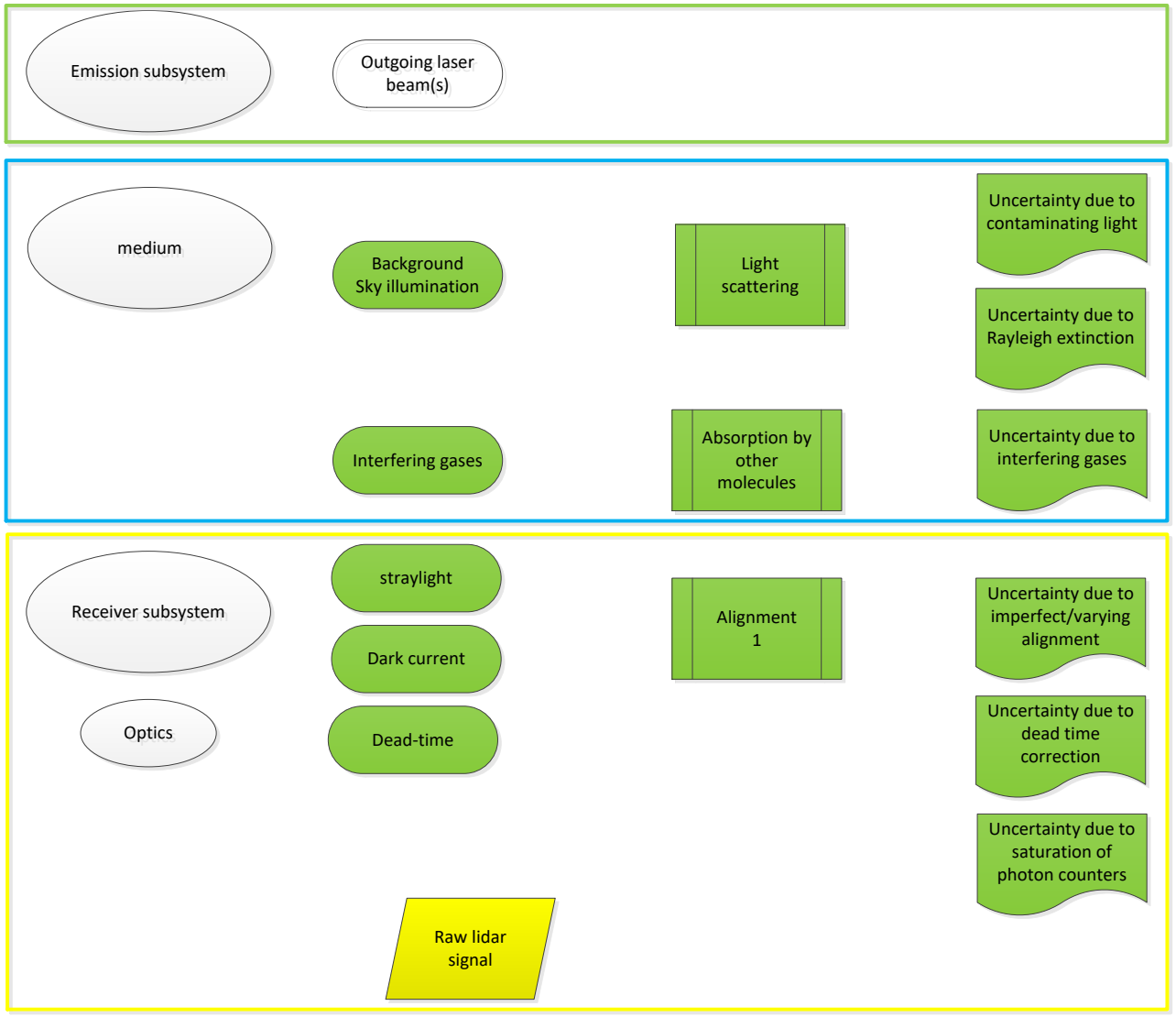

Figure 5. Three elements are shown in the physical part of the PTU chain: the emitter box (outlined by the green rectangle), the medium corresponding to the atmosphere (blue rectangle), the receiver box with e.g. the optics and detectors (yellow rectangle). The processing software part is shown in Figure 6. Processes, components and uncertainties that are dealt with are printed as filled green shapes. Items that are numbered following the discussion in the Element contribution section (5).

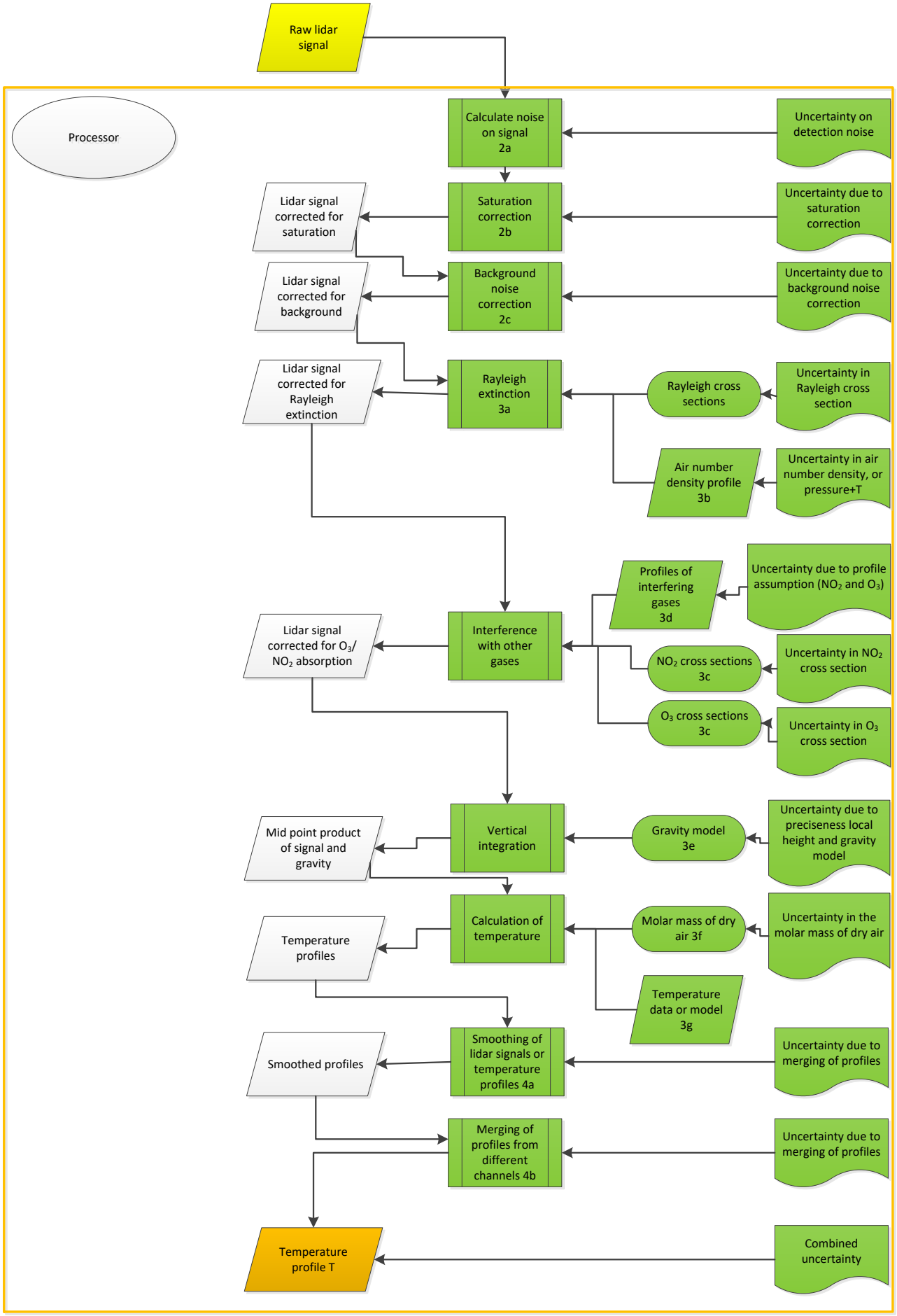

Figure 6. Continuation of Figure 5 with the processing software steps.

5 Element contributions

5.1 Alignment (1)

The correct alignment of the lidar system, that is the alignment of the laser beam with the receiving system and of the telescope with the optics of filtering system, is ensured by specific tests, as for instance developed in the framework of the EARLINET quality assurance program. In particular, the telecover test and the Rayleigh fit test are performed to check and correct the alignment of the lidar system in the near range (planetary bondary layer) and in the far range (free troposphere or above), respectively – see Freudenthaler et al. (2018).

For each lidar system there is a certain degree of misalignment between the laser beam and the receiving system due to residual uncertainties in the telecover and Rayleigh fit tests or possible mechanical/thermal instabilities of the optical and mechanical components forming both transmission and receiving systems. The misalignment of a lidar system changes the angle on the receiver of the backscattered light at each altitude level, which affects the overlap function. Most temperature lidar systems start at relatively high altitudes and then there is usually a full overlap.

Information / data	Type / value / equation	Notes / description
Name of effect	Alignment	
Contribution identifier	1	
Measurement equation parameter(s) subject to effect	η	In Eq. 1
Contribution subject to effect (final product or sub-tree intermediate product)	Lidar signal P	Eq. 1
Time correlation extent & form	Various time scales	Extent & form not quantified
Other (non-time) correlation extent & form	1) Possible correlation with vertical range 2) Possible correlation with the temperature of components forming both transmission and receiving systems during measurements	Extent & form not quantified
Uncertainty PDF shape	N/A	Systematic effect
Uncertainty & units	0% (relative uncertainty)	Assumed to be negligible for a well maintained system
Sensitivity coefficient	<1	Assumed that only data not effected is reported
Correlation(s) between affected parameters	None	
Element/step common for all sites/users?	Yes	
Traceable to ...	No	
Validation	Keckhut et al., 1993	

5.2 Pre-processing (2)

5.2.1 Detection noise (2a)

Random noise is inherently present in any physical system performing an actual measurement. Signal detection uncertainty is introduced at the detection level, where the signal is recorded in the data files (raw signal *R*). It is derived from Poisson statistics associated with the probability of detection of a repeated random event (Type-A uncertainty estimation). Using the subscript "(*DET*)" for "detection noise", the uncertainty in the raw (summed) signal *R* due to detection noise expressed for each altitude bin k and for a single temperature channel is written:

$$u_{R(DET)}(k) = \sqrt{R(k)} \tag{20}$$

There is no correlation between any of the samples considered as this uncertainty component is due to purely random effects (signal detection). It is propagated to the retrieved temperature profile by systematically assigning the individual input quantities covariance matrix's non-diagonal terms to zero. Assuming a non-paralyzable photon-counting hardware, this uncertainty component is therefore propagated to the saturation and background noise-corrected signal *P* by converting Eq. (9):

$$u_{P(DET)}(k) = \left(\frac{P(k)}{R(k)}\right)^2 \sqrt{R(k)} \tag{21}$$

This uncertainty component is then propagated to the lidar-derived relative density *N* by:

$$u_{N(DET)}(k) = \frac{N(k)}{P(k)} u_{P(DET)}(k) \tag{22}$$

Next, it is propagated through Eq. (11) assuming that the signals are uncorrelated between two consecutive altitudes:

$$u_{\overline{N}(DET)}(k') = \frac{1}{2}\sqrt{\frac{N(k'+1)}{N(k')} u^2_{N(DET)}(k') + \frac{N(k')}{N(k'+1)} u^2_{N(DET)}(k'+1)} \tag{23}$$

The detection noise uncertainty then needs to be propagated to the sum S defined in Eq. (12). This sum involves correlated terms as two consecutive terms contain two occurrences of the same values (*k′* and *k′+1* first level, then *k′+1* and *k′+2* next level, etc.).

$$u_{S(DET)}(k) = \sqrt{\sum_{k'=k}^{kTOP-1} \overline{g}^{-2}(k') u^2_{\overline{N}(DET)}(k') + 2 \sum_{k'=k}^{kTOP-2} \sum_{k''=k'}^{KTOP-1} g(k') g(k'') u_{\overline{N}(DET)}(k') u_{\overline{N}(DET)}(k'') r_{k'k''}} \tag{24}$$

The correlation coefficients $r_{k'k''}$ between the terms $\overline{N}(k')$ and $\overline{N}(k'')$ are not strictly known. However, with the realistic assumption that the values of two consecutive terms are almost equal (i.e., *N* values, *g* values and $u_{N(DET)}$ values), the equation above can be simplified to:

$$u_{S(DET)}(k) = \sqrt{2 \sum_{k'=k}^{kTOP-1} \overline{g}^{-2}(k') u^2_{\overline{N}(DET)}(k')} \tag{25}$$

This expression is different from an expression assuming that all terms are independent (it is a factor of $\sqrt{2}$ larger), and it is also different from an expression assuming that all the terms are fully correlated (the weighed sum of all individual uncertainties).

Finally, the temperature uncertainty due to detection noise $u_{T(DET)}$ is computed for the density integration:

$$u_{T(DET)}(k) = \frac{1}{N(k)T(k)} \sqrt{T^2(k) u^2_{N(DET)}(k) + T_a^2(k_{TOP}) u^2_{N(DET)}(k_{TOP}) + \left(\frac{M_a \delta z}{R_a}\right)^2 u^2_{S(DET)}(k)} \tag{26}$$

The temperature uncertainty due to detection noise can be of any order of magnitude, depending on

altitude and lidar performance and/or specification such as signal magnitude, emission wavelength, vertical sampling, and the duration of temporal integration. In general, the temperature uncertainty increases with an e-folding rate (of about 14 km) as a function of signal magnitude and of altitude.

Information / data	Type / value / equation	Notes / description
Name of effect	Detection noise	
Contribution identifier	2a	
Measurement equation parameter(s) subject to effect	R	Eq. 9
Contribution subject to effect (final product or sub-tree intermediate product)	T	Eq.19
Time correlation extent & form	Various time scales (structured random)	Will change with each measurement session due to varying experimental conditions
Other (non-time) correlation extent & form	Vertical smoothing/spatial resolution	
Uncertainty PDF shape	Poisson/normal	
Uncertainty & units	Large (>1 K) at the top of profile, decreasing downwards to a minimal uncertainty at the bottom of the profile	
Sensitivity coefficient	1	
Correlation(s) between affected parameters	Not applicable	
Element/step common for all sites/users?	Yes	
Traceable to ...	Leblanc et al., 2016d	
Validation	Simoneov et al., 1999	

5.2.2 Saturation (pulse pile-up) correction (2b)

This uncertainty component is introduced only for channels operating in photon-counting mode. If we consider a non-paralyzable counting hardware, the only input quantity to introduce is the hardware's dead time (sometimes called resolving time), which characterizes the speed of the counting electronics. The dead time τ and its uncertainty u_τ are generally among the technical specifications provided by the hardware manufacturer (Type-B estimation).

This uncertainty component is introduced where the signal is recorded in the data files (raw signal *R*). Using the subscript "(*SAT*)" for "saturation", the saturation correction uncertainty propagated to the saturation and background noise-corrected signal *P* is obtained:

$$u_{P(SAT)}(k) = \frac{2\delta z}{cL} P^2(k) u_\tau \tag{27}$$

Just like the detection noise component, the saturation correction uncertainty component is propagated to the lidar-derived relative density *N*:

$$u_{N(SAT)}(k) = \frac{N(k)}{P(k)} u_{P(SAT)}(k) \tag{28}$$

The saturation correction is applied to the lidar signals consistently at all altitudes. Its uncertainty is therefore propagated assuming full correlation between two consecutive altitudes *z(k')* and *z(k'+1)*.

$$u_{\overline{N}(SAT)}(k') = \frac{\overline{N}(k')}{2}\left(\frac{u_{N(SAT)}(k')}{N(k')} + \frac{u_{N(SAT)}(k'+1)}{N(k'+1)}\right) \tag{29}$$

The saturation correction uncertainty then propagates to the sum *S* defined in Eq. (12) assuming again full correlation between altitude bins:

$$u_{S(SAT)}(k) = \sum_{k'=k}^{kTOP-1} g(k') u_{\overline{N}(SAT)}(k') \tag{30}$$

Finally, the temperature uncertainty due to saturation correction $u_{T(SAT)}$ is for the density integration with the same full correlation assumptions:

$$u_{T(SAT)}(k) = \frac{1}{N(k)}\left| T(k) u_{N(SAT)}(k) - T_a(k_{TOP}) u_{N(SAT)}(k_{TOP}) - \frac{M_a \delta z}{R_a} u_{S(SAT)}(k) \right| \tag{31}$$

Information / data	Type / value / equation	Notes / description
Name of effect	Saturation correction	
Contribution identifier	2b	
Measurement equation parameter(s) subject to effect	P	Eq.9
Contribution subject to effect (final product or sub-tree intermediate product)	T	Eq.19
Time correlation extent & form	Various time scales (structured random)	Will change with each measurement session due to varying experimental conditions
Other (non-time) correlation extent & form	N/A	
Uncertainty PDF shape	Poisson/normal	
Uncertainty & units	Can be large (~1 K) at bottom of profile, rapidly decreasing with decreasing signal strength	Depends on the used setup, photon counters and signal intensity
Sensitivity coefficient	1	

Correlation(s) between affected parameters	Not applicable	
Element/step common for all sites/users?	yes	
Traceable to ...	Leblanc et al., 2016d	
Validation	Donovan et al, 2003 Bristow, 1998	

5.2.3 Background noise extraction (2c)

At far range, the backscattered signal is too weak to be detected and any non-zero signal reflects the presence of undesired skylight or electronic background noise. This background noise is typically subtracted from the total signal by fitting the uppermost part of the lidar signal with a linear or non-linear function of altitude *B*. A new uncertainty component associated with the noise fitting procedure must therefore be introduced. Here we provide a detailed treatment for the simple case of a linear fit. It can be easily generalized to many other fitting functions. The linear fitting function takes the form:

$$B(k) = b_0 + b_1 z(k) \tag{32}$$

For many well-known fitting methods (e.g., least-squares), the fitting coefficients b_i can be calculated analytically together with their uncertainty u_{bi} and their correlation coefficient rb_i,b_j (Type-A estimation) (Press et al., 1986). Using the subscript "(*BKG*)" for "background noise", the background noise correction uncertainty can then be introduced by

$$u_{P(BKG)}(k) = \sqrt{u_{b0}^2 + u_{b1}^2 z^2(k) + 2z(k)\,\mathrm{cov}(b_0, b_1)} \tag{33}$$

The above expression can be expanded and/or modified based on the actual form of the fitting function, and taking into account the fitting coefficients' covariance matrix returned by the fitting routine. Just like the saturation correction uncertainty, the uncertainty component due to the background noise extraction can be propagated through the temperature retrieval assuming full correlation in altitude:

$$u_{N(BKG)}(k) = \frac{N(k)}{P(k)} u_{P(BKG)}(k) \tag{34}$$

$$u_{\overline{N}(BKG)}(k') = \frac{\overline{N}(k')}{2}\left(\frac{u_{N(BKG)}(k')}{N(k')} + \frac{u_{N(BKG)}(k'+1)}{N(k'+1)}\right) \tag{35}$$

$$u_{S(BKG)}(k) = \sum_{k'=k}^{kTOP-1} g(k') u_{\overline{N}(BKG)}(k') \tag{36}$$

$$u_{T(BKG)}(k) = \frac{1}{N(k)}\left|T(k)u_{N(BKG)}(k) - T_a(k_{TOP})u_{N(BKG)}(k_{TOP}) - \frac{M_a \delta z}{R_a} u_{S(BKG)}(k)\right| \tag{37}$$

The order of magnitude of this uncertainty component depends on the magnitude of the background noise, and if signal-induced noise is present, on the slope of this noise with respect to the signal slope. In general, a systematic pattern which consists of a rapid increase in the first 3-4 km below the tie-on altitude as density is integrated downward can be seen, followed by a decrease as we get further and further from the tie-on altitude. The e-folding rate is about 7 km for the entire family of curves, which reflects the main influence of the 1/*N* term in Eq. (37). The temperature uncertainty maximum is larger when the magnitude of the noise is larger.

Information / data	Type / value / equation	Notes / description
Name of effect	Background noise correction	
Contribution identifier	2c	
Measurement equation parameter(s) subject to effect	B(k)	Eq. 9
Contribution subject to effect (final product or sub-tree intermediate product)	T	

Time correlation extent & form	Various time scales (structured random)	Will change with each measurement session due to varying experimental conditions, e.g. sky brightness, dark current
Other (non-time) correlation extent & form	Not applicable	
Uncertainty PDF shape	Poisson/normal	
Uncertainty & units	<0.3 K	
Sensitivity coefficient	1	
Correlation(s) between affected parameters	Not applicable	
Element/step common for all sites/users?	Yes	
Traceable to ...	Leblanc et al., 2016d	
Validation	Keckhut et al., 1993 Leblanc et al., 1998	

5.3 External inputs (3)

5.3.1 Rayleigh extinction cross section (3a)

All lidar-derived relative density uncertainty components due to the atmospheric extinction are computed starting from Eq. (10). The Rayleigh extinction cross-sections at the emitted and received wavelengths are among the input quantities. Their values typically originate from theoretical calculations assuming a given atmospheric composition (see for example Bates, 1984; Eberhard, 2010), and can be assumed constant with altitude (well-mixed atmosphere). A review of the different calculations and the associated uncertainties can be found in Leblanc et al. (2016d, Appendix D and section 3.5 therein). The uncertainty, as reported in the literature, is either due to random or systematic effects, or both. These two types of uncertainty are not introduced and propagated identically in the lidar temperature measurement model. The subscripts suffix "*Rand*" (for "random") and "*Sys*" (for "systematic") are used hereafter to make this distinction.

5.3.1.1 Relative density uncertainty for Rayleigh backscatter channels

For Rayleigh backscatter channels, the received wavelength (λ_R) is identical to the emitted wavelength (λ_E), and the cross-section uncertainty due to random and systematic effects is introduced and propagated identically throughout the temperature retrieval. Using the subscript "(σM)" for "molecular extinction cross-section" uncertainty component, and the suffixes "*Rand*" and "*Sys*" for random and "systematic" components respectively, the Rayleigh extinction cross-section uncertainty due to random and systematic effects can be propagated to the lidar-derived relative density N:

$$u_{N(\sigma MX)}(k) = 2N(k)\delta z\sum_{k'=0}^{k} N_a(k')u_{\sigma M\_E\_X} \quad \text{with } X\text{=}Rand, Sys \tag{38}$$

5.3.1.2 Relative density uncertainty for Raman backscatter channels

For Raman backscatter channels (Strauch et al., 1971), the received and emitted wavelengths are different, and the cross-section uncertainty due to random and systematic effects are introduced and propagated differently. The uncertainty component due to random effect is computed as:

$$u_{N(\sigma MR)}(k) = N(k)\delta z\sum_{k'=0}^{k} N_a(k')\sqrt{u^2_{\sigma M\_E\_Rand} + u^2_{\sigma M\_R\_Rand}} \tag{39}$$

The uncertainty component due to systematic effects is computed as:

$$u_{N(\sigma MS)}(k) = N(k)\delta z\sum_{k'=0}^{k} N_a(k')\left(u_{\sigma M\_E\_Sys} + u_{\sigma M\_R\_Sys}\right) \tag{40}$$

5.3.1.3 Propagation to temperature

For both Rayleigh and Raman backscatter, both random and systematic components of the lidar-derived relative density uncertainty due to Rayleigh extinction cross-sections are propagated to temperature similarly to the saturation and background uncertainty components:

$$u_{\overline{N}(\sigma MX)}(k') = \frac{\overline{N}(k')}{2}\left(\frac{u_{N(\sigma MX)}(k')}{N(k')} + \frac{u_{N(\sigma MX)}(k'+1)}{N(k'+1)}\right) \quad \text{with } X\text{=}Rand, Sys \tag{41}$$

$$u_{S(\sigma MX)}(k) = \sum_{k'=k}^{kTOP-1} g(k')u_{\overline{N}(\sigma MX)}(k') \quad \text{with } X\text{=}Rand, Sys \tag{42}$$

$$u_{T(\sigma MX)}(k) = \frac{1}{N(k)}\left|T(k)u_{N(\sigma MX)}(k) - T_a(k_{TOP})u_{N(\sigma MX)}(k_{TOP}) - \frac{M_a\delta z}{R_a}u_{S(\sigma MX)}(k)\right| \quad \text{with } X\text{=}Rand, Sys \tag{43}$$

Information / data	Type / value / equation	Notes / description
Name of effect	Rayleigh extinction cross sections	
Contribution identifier	3a	
Measurement equation parameter(s) subject to effect	$\Delta\sigma_M$	Eq. 10
Contribution subject to effect (final product or sub-tree intermediate product)	T	Eq. 11
Time correlation extent & form	None	
Other (non-time) correlation extent & form	None	
Uncertainty PDF shape	Unknown	
Uncertainty & units	Large (~1 K) at bottom of profile	See line numbered 4 in Figure 8 for an example of how it changes with altitude
Sensitivity coefficient	1	
Correlation(s) between affected parameters	Not applicable	
Element/step common for all sites/users?	Yes	
Traceable to ...	Leblanc et al., 2016d	
Validation	She et al., 1992	

5.3.2 Uncertainty owing to air number density, temperature and pressure profiles (3b)

An external, a priori profile of air number density (N_a) is needed to correct for Rayleigh extinction as formulated in Eq. (10). Air number density is generally not estimated directly, but rather derived from air temperature and pressure. Below we discuss the propagation of uncertainty for both ways of obtaining air number density.

5.3.2.1 *Estimation from an air number density profile*

Here, it is assumed that the air density profile N_a is made of fully-correlated values in altitude. If air number density is not derived from air temperature and pressure, its uncertainty u_{Na} is propagated to the lidar-derived relative density by:

$$u_{N(Na)}(k) = N(k)\delta z\left(\sigma_{M\_E} + \sigma_{M\_R}\right)\sum_{k'=0}^{k} u_{Na}(k') \tag{44}$$

This component is then propagated to temperature using the same approach as for saturation and background noise correction uncertainties.

5.3.2.2 *Estimation from an air temperature and pressure profile*

When the ancillary number density is computed from an ancillary temperature T_a and pressure p_a source (e.g., radiosonde measurements or meteorological models), the uncertainties u_{Ta} and u_{pa} must be introduced and the degree of correlation between temperature and pressure must be estimated.

If temperature and pressure are measured or computed independently, then the complete covariance matrix in the vertical dimension needs to be estimated. This is the most complex case to consider because of the interplay between the lack of correlation between T_a and p_a at any given altitude, and the high correlation between the temperature values at two consecutive altitudes, or between the pressure values at two consecutive altitudes. However, a good approximation consists of considering the propagation linearly, i.e., first combining the uncertainties at one fixed level assuming no correlation, and then propagating the combined uncertainty assuming full correlation between two consecutive altitudes. In this case, the lidar-derived relative density uncertainty due to the ancillary air number density can be written:

$$u_{N(Na)}(k) = N(k)\delta z\sum_{k'=0}^{k}\left(\sigma_{M\_E} + \sigma_{M\_R}\right)N_a(k')\sqrt{\frac{u_{pa}^2(k')}{p_a^2(k')} + \frac{u_{Ta}^2(k')}{T_a^2(k')}} \tag{45}$$

If temperature and pressure are known to be fully correlated, then, the lidar-derived relative density uncertainty due to the ancillary air number density becomes:

$$u_{N(Na)}(k) = N(k)\delta z\sum_{k'=0}^{k}\left(\sigma_{M\_E} + \sigma_{M\_R}\right)N_a(k')\left|\frac{u_{pa}(k')}{p_a(k')} - \frac{u_{Ta}(k')}{T_a(k')}\right| \tag{46}$$

5.3.2.3 *Propagation to the temperature profile*

The lidar-derived number density uncertainty due to ancillary air number density is propagated to temperature assuming full correlation in altitude:

$$u_{\overline{N}(Na)}(k') = \frac{\overline{N}(k')}{2}\left(\frac{u_{N(Na)}(k')}{N(k')} + \frac{u_{N(Na)}(k'+1)}{N(k'+1)}\right) \tag{47}$$

$$u_{S(Na)}(k) = \sum_{k'=k}^{kTOP-1} g(k')u_{\overline{N}(Na)}(k') \tag{48}$$

$$u_{T(Na)}(k) = \frac{1}{N(k)}\left|T(k)u_{N(Na)}(k) - T_a(k_{TOP})u_{N(Na)}(k_{TOP}) - \frac{M_a\delta z}{R_a}u_{S(Na)}(k)\right| \tag{49}$$

Information / data	Type / value / equation	Notes / description
Name of effect	External air number density, temperature and pressure profiles	This table corresponds to the entire section 5.3.2
Contribution identifier	3b	
Measurement equation parameter(s) subject to effect	N	Eq. 10
Contribution subject to effect (final product or sub-tree intermediate product)	T	Eq. 11
Time correlation extent & form	Various time scales (structured random)	Will change with each measurement session due to varying experimental conditions
Other (non-time) correlation extent & form	altitude	
Uncertainty PDF shape		
Uncertainty & units	Largest (<0.2 K) at bottom of profile	See line numbered 5 in Figure 8
Sensitivity coefficient	1	
Correlation(s) between affected parameters		
Element/step common for all sites/users?	yes	
Traceable to ...	Leblanc et al., 2016d	
Validation	Leblanc et al., 1998	

5.3.4 Interfering gases' cross sections (3c)

Temperature-dependent ozone and NO_2 absorption cross-section values typically can be found in published works originating from spectroscopy groups around the world (e.g., Brion et al., 1998; Bogumil et al., 2003; Chehade et al., 2013; Gorshelev et al., 2014; Burkholder and Talukdar, 1994; Burrows et al., 1999; Vandaele et al., 1998). The random component of the cross-section uncertainty is normally provided in these works. Occasionally, one or more components due to systematic effects are also provided. For the ozone absorption cross-section, a review and assessment of the available datasets is summarized Leblanc et al. (2016d). Just like for Rayleigh extinction cross-sections, these two types of components are not introduced and propagated identically in the lidar temperature measurement model. The formulation of their propagation is identical to that just presented for Rayleigh extinction cross-sections, except that the air number density is replaced by the interfering gas number density, and the cross-section uncertainty is now a function of temperature, i.e., altitude. For Rayleigh backscatter channels:

$$u_{N(\sigma igX)}(k) = 2N(k)\delta z\sum_{k'=0}^{k} N_{O3}(k')u_{\sigma ig\_1X}(k') \quad \text{with } ig = O_3, NO_2 \text{ and } X=Rand, Sys \tag{50}$$

For Raman backscatter channels:

$$u_{N(\sigma igRand)}(k) = N(k)\delta z\sqrt{\sum_{k'=0}^{k} N_{ig}^2(k')\left(u_{\sigma ig\_E\_Rand}^2(k') + u_{\sigma ig\_R\_Rand}^2(k')\right)} \quad \text{with } ig = O_3, NO_2 \tag{51}$$

$$u_{N(\sigma igS)ys}(k) = N(k)\delta z\sum_{k'=0}^{k} N_a(k')\left(u_{\sigma ig\_E\_Sys}(k') + u_{\sigma ig\_R\_Sys}(k')\right) \quad \text{with } ig = O_3, NO_2 \tag{52}$$

Their propagation to temperature can then be written:

$$u_{\bar{N}(\sigma igX)}(k') = \frac{\bar{N}(k')}{2}\left(\frac{u_{N(\sigma igX)}(k')}{N(k')} + \frac{u_{N(\sigma igX)}(k'+1)}{N(k'+1)}\right) \quad \text{with } ig = O_3, NO_2 \text{ and } X=Rand, Sys \tag{53}$$

$$u_{S(\sigma igX)}(k) = \sum_{k'=k}^{kTOP-1} g(k')u_{\bar{N}(\sigma igX)}(k') \quad \text{with } ig = O_3, NO_2 \text{ and } X=Rand, Sys \tag{54}$$

$$u_{T(\sigma igX)}(k) = \frac{1}{N(k)}\left|T(k)u_{N(\sigma igX)}(k) - T_a(k_{TOP})u_{N(\sigma igX)}(k_{TOP}) - \frac{M_a\delta z}{R_a}u_{S(\sigma igX)}(k)\right| \quad ig = O_3, NO_2; X=Rand, Sys \tag{55}$$

The contribution of ozone absorption to uncertainty in the temperature profiles is larger in the visible (532 nm and 607 nm which are both in the Chappuis band) than in the ultraviolet (355 nm and 387 nm). Conversely, the contribution of NO_2 absorption is larger for ultraviolet wavelengths than for wavelengths in the visible domain.

Information / data	Type / value / equation	Notes / description
Name of effect	Interfering gases' cross section differential	
Contribution identifier	3c	
Measurement equation parameter(s) subject to effect	$\Delta\sigma_{ig}$	Eq. 11
Contribution subject to effect (final product or sub-tree intermediate product)	N	Eq. 11
Time correlation extent & form	None	
Other (non-time) correlation extent & form		
Uncertainty PDF shape		

Uncertainty & units	For ozone: up to 1 K error if neglected when working in the Chappuis band (e.g., 532 nm and 607 nm) For NO_2: up to a 0.2 K error if neglected at 355 nm and 387 nm	Depends on the quantity and profile of the interfering gas and wavelength used for retrieval.
Sensitivity coefficient	1	
Correlation(s) between affected parameters		
Element/step common for all sites/users?	yes	
Traceable to ...	Leblanc et al., 2016d	
Validation	Sica et al., 2001	for ozone retrievals with the 532 and 589 nm wavelengths (contribution of ozone is negligible around 350 nm) At this moment NO_2 is not yet corrected for, although it is recommended.

5.3.5 Interfering gases' atmospheric profiles (3d)

The ozone and NO_2 absorption terms in Eq. (10) form the sum of a priori ozone and NO_2 number densities taken at all altitudes from the ground to the altitude considered *z(k)*. Depending on the data source, these ancillary profiles may be mixing ratio or number density (Ahmad et al., 1987; Bauer et al., 2012; Bracher et al., 2005; Brohede et al., 2007) Assuming that all values within the same ancillary profile are fully correlated, uncertainty components due to the ancillary ozone and NO_2 profiles can be propagated to temperature similarly to the uncertainty component due to air number density:

$$u_{N(Nig)}(k) = N(k)\sum_{k'=0}^{k}\left(\sigma_{ig\_E}(k') + \sigma_{ig\_R}(k')\right)u_{Nig}(k') \text{ with } ig = O_3, NO_2 \tag{56}$$

$$u_{\overline{N}(Nig)}(k') = \frac{\overline{N}(k')}{2}\left(\frac{u_{N(Nig)}(k')}{N(k')} + \frac{u_{N(Nig)}(k'+1)}{N(k'+1)}\right) \tag{57}$$

$$u_{S(Nig)}(k) = \sum_{k'=k}^{kTOP-1}\overline{g}(k')u_{\overline{N}(Nig)}(k') \tag{58}$$

$$u_{T(Nig)}(k) = \frac{1}{N(k)}\left|T(k)u_{N(Nig)}(k) - T_a(k_{TOP})u_{N(Nig)}(k_{TOP}) - \frac{M_a\delta z}{R_a}u_{S(Nig)}(k)\right| \tag{59}$$

The contribution of ozone is larger for visible wavelengths than in the UV, and the contribution of NO_2 is larger for ultraviolet wavelengths than in the visible.

Information / data	Type / value / equation	Notes / description
Name of effect	Interfering gases' atmospheric profiles	
Contribution identifier	3d	
Measurement equation parameter(s) subject to effect	N_{ig}	Eq. 10
Contribution subject to effect (final product or sub-tree intermediate product)	N	
Time correlation extent & form	Various time scales	Will change with each measurement session due to varying experimental conditions in terms of atmospheric composition
Other (non-time) correlation extent & form	None	
Uncertainty PDF shape	Poisson/normal	
Uncertainty & units	For ozone: up to 1 K error if neglected when working in the Chappuis band (e.g., 532 nm and 607 nm) For NO_2: depending on NO_2 density, but up to a 0.2 K error if neglected at 355 nm and 387 nm	
Sensitivity coefficient	1	
Correlation(s) between affected parameters	None	

Element/step common for all sites/users?	Yes	
Traceable to ...	Leblanc et al., 2016d	
Validation	Faduilhe et al., 2005 -	For ozone The NO_2-correction is recommended but not yet implemented in the current lidar products.

5.3.6 Acceleration of gravity (3e)

The acceleration of gravity is an input quantity introduced in Eq. (12). The constants g_0, g_1 and g_2 relate to the Earth's geometry and to the geodetic latitude of the lidar site. If a value of the local ellipsoid height at the lidar site *h(0)* is not known, we can approximate it to the site's altitude above mean sea level *z(0)*. For all altitude-dependent and latitude-dependent formulations of the acceleration of gravity, the difference between *h(0)* and *z(0)* is by far the largest source of error in the computation of the acceleration of gravity. We therefore can define a new uncertainty component uh associated with the approximation of *h*. The values of *h* at neighboring altitudes are fully correlated, and their standard uncertainty can be deduced directly from Eq. (15):

$$u_{\bar{h}}(k') = \frac{1}{2}\left(u_h(k') + u_h(k'+1)\right) \tag{62}$$

The height uncertainty is then propagated to temperature:

$$u_{T(g)}(k) = \frac{1}{N(k)} \frac{M_a \delta z}{R_a} g_0 \sum_{k'=k}^{kTOP-1} \bar{N}(k')\left(g_1 + 2g_2 \bar{h}(k')\right) u_{\bar{h}}(k') \tag{63}$$

The relative uncertainty in the temperature profiles is therewith directly related to the relative uncertainty in gravity. An example is given in Figure 7 below, where the altitude-dependence of gravity is considered, but latitude not. Deviations in the temperature profiles depend on the assumed and true latitude as well as on altitude, and can reach up to 0.7 K. Similar simulations have been carried out for the case where gravity is treated as a constant (both altitude-dependence and latitude-dependence neglected). There up to 6 K deviations are found.

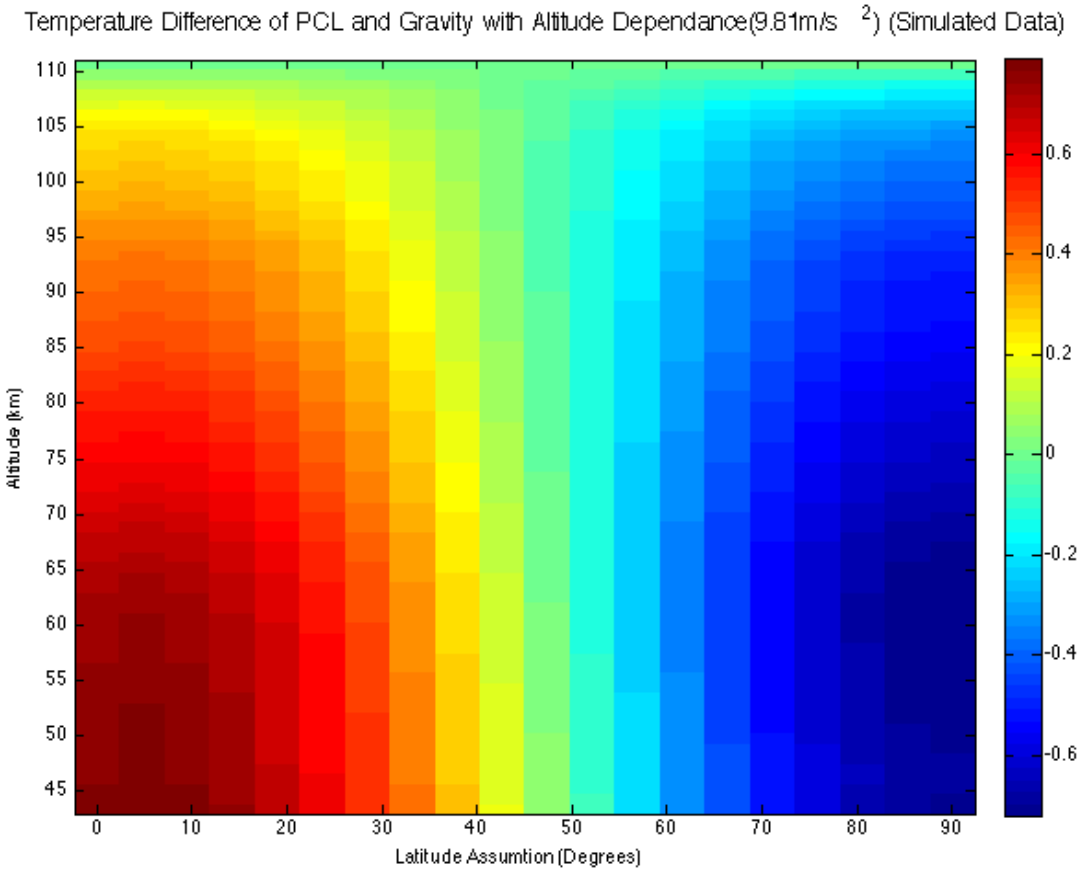

Figure 7. Effect of disregarding the contribution of latitude to gravity taking the altitude-dependence of gravity into account. The gravity is simulated here for a latitude of 45 degrees. The offset in temperature then depends on the latitude of the site (horizontal axis) and the altitude (vertical axis). Simulations and figure prepared by professor R. Sica, PI of the Purple Crow lidar (Western university, Ontario, Canada).

Information / data	Type / value / equation	Notes / description
Name of effect	Acceleration of gravity	
Contribution identifier	3e	
Measurement equation parameter(s) subject to effect	G	Eq. 12
Contribution subject to effect (final product or sub-tree intermediate product)	S	Eq.12
Time correlation extent & form	None	
Other (non-time) correlation extent & form	Geolocation of instrument	
Uncertainty PDF shape	N/A	
Uncertainty & units	<0.2 K if altitude- and latitude-dependent gravity is used which is the case for the systems described.	
Sensitivity coefficient	1	
Correlation(s) between affected parameters		
Element/step common for all sites/users?	yes	
Traceable to ...	Leblanc et al., 2016d	
Validation	Sica and Haefele., 2015	

5.3.7 Molecular mass of air (3f)

The molecular mass of dry air M_a is introduced in Eq. (11). Its uncertainty u_{Ma}, can be propagated to temperature using:

$$u_{T(Ma)}(k) = \frac{\delta z}{R_a} \frac{S(k)}{N(k)} u_{Ma} \quad (60)$$

The uncertainty introduced by this component remains negligible below 90 km, which is above the highest altitude reported by most lidar systems, and it has a variation with altitude similar to that due to acceleration of gravity. According to Keckhut et al. (1993), the dissociation of oxygen should lead to a 2% correction at 100 km and 7% correction at 110 km. The lidar systems used here do not report temperatures at these altitudes.

Information / data	Type / value / equation	Notes / description
Name of effect	Molecular mass of air	
Contribution identifier	3f	
Measurement equation parameter(s) subject to effect	M_a	Eq. 11
Contribution subject to effect (final product or sub-tree intermediate product)	T	Eq.11
Time correlation extent & form	Various time scales	
Other (non-time) correlation extent & form	None	
Uncertainty PDF shape	N/A	
Uncertainty & units	<0.1 K when altitude is below 90 km. Increasingly important with altitude above	
Sensitivity coefficient	1	
Correlation(s) between affected parameters		
Element/step common for all sites/users?	Yes	
Traceable to ...	Leblanc et al., 2016d	
Validation	Keckhut et al., 1993 Argall, 2007	

5.3.8 External temperature for tie-on at the top of the profile (3g)

An external or ancillary temperature value *T*a at altitude $z(k_{TOP})$ is needed to initialize the profile at the top. Using the subscript "(*TIE*)" for "tie-on", the ancillary temperature uncertainty $u_{Ta(kTOP)}$ is propagated to the retrieved temperature profile):

$$u_{T(TIE)}(k) = \frac{N(k_{TOP})}{N(k)} u_{Ta}(k_{TOP}) \quad (61)$$

The uncertainty due to ancillary temperature is reduced downward with altitude with an approximate e-folding rate of 7 km due to the term 1/N in the equation above.

Information / data	Type / value / equation	Notes / description
Name of effect	Tie-on temperature	
Contribution identifier	3g	
Measurement equation parameter(s) subject to effect	Ta(k_{TOP})	Eq. 11
Contribution subject to effect (final product or sub-tree intermediate product)	T	Eq. 11
Time correlation extent & form	Various time scales (structured random)	Will change with each measurement session due to varying experimental conditions.
Other (non-time) correlation extent & form		
Uncertainty PDF shape	N/A	
Uncertainty & units	Negligible from 20 km below tie-on altitude	Depends on uncertainty of the external temperature and whether data are reported up to tie-on temperature.
Sensitivity coefficient	1	
Correlation(s) between affected parameters	None	
Element/step common for all sites/users?	Yes	When using the density integration technique
Traceable to ...	Leblanc et al., 2016d	
Validation	Leblanc et al., 1998	

5.4 Spatio-temporal integration (4)

5.4.1 Propagation of uncertainty when vertically filtering (smoothing) the lidar signal or temperature profile (4a)

The smoothing procedure was introduced as an optional step in the measurement model and is applied either to the lidar signal or to the retrieved temperature profile for the instruments targeted for GaiaClim.

5.4.1.1 Smoothing the lidar signal before the temperature profile is computed

From Eq. (16) and using the same notations, the uncertainty component due to detection noise is propagated to the smoothed signal profile assuming no correlation between the neighbouring points:

$$u_{sm(DET)}(k) = s_m(k)\sqrt{\sum_{p=-n}^{n} c_p^2(k)\frac{u_{s(DET)}^2(k+p)}{s^2(k+p)}} \tag{62}$$

For all other uncertainty components except temperature tie-on, acceleration of gravity, and the molecular mass of air, full correlation is assumed between the neighbouring points, and the uncertainty in the smoothed signal can be written:

$$u_{sm(X)}(k) = s_m(k)\sum_{p=-n}^{n} c_p(k)\frac{u_{s(X)}(k+p)}{s(k+p)} \tag{63}$$

with X = SAT, BKG, σ_{MR}, σ_{MS}, N_a, σ_{igR}, σ_{igS}, N_{ig}.

The uncertainty components due to temperature tie-on, acceleration of gravity, and the molecular mass of air are not included in the above expression because they are introduced later in the data processing. In this case, the respective equations in sections 5.3.6 to 5.3.8 apply directly to the temperature profile retrieved from the smoothed lidar-derived number density.

5.4.1.2 Smoothing the retrieved temperature profile

The temperature uncertainty components due to detection noise are propagated to the smoothed temperature profile assuming no correlation between neighbouring points:

$$u_{Tm(DET)}(k) = \sqrt{\sum_{p=-n}^{n} c_p^2(k)u_{T(DET)}^2(k+p)} \tag{64}$$

For all other uncertainty components, full correlation is assumed between the two channels:

$$u_{Tm(X)}(k) = \sum_{p=-n}^{n} c_p(k)u_{T(X)}(k+p) \tag{65}$$

with *X = SAT, BKG ,σMR, σMS, Na, σigR, σigS, Nig, g, TTOP, Ma.*

Information / data	Type / value / equation	Notes / description
Name of effect	Vertical filtering	
Contribution identifier	4a	
Measurement equation parameter(s) subject to effect	P or T	Eq.9 or Eq. 11
Contribution subject to effect (final product or sub-tree intermediate product)	T_m	Eq. 17
Time correlation extent & form	None	

Other (non-time) correlation extent & form		
Uncertainty PDF shape		
Uncertainty & units	Up to 2 K	Depending on the filter type used, the number of altitude bins used and the shape of the profile
Sensitivity coefficient	1	
Correlation(s) between affected parameters		
Element/step common for all sites/users?	Yes, but optional	
Traceable to ...	Leblanc et al., 2016d	
Validation	Leblanc et al., 1998	

5.4.2 Propagation of uncertainty when merging multiple channels together (4b)

The merging procedure was again introduced as an optional step in the measurement model. If present it can be applied either to the lidar signals or the temperature profiles. For the chosen sites, merging is applied.

5.4.2.1 Merging lidar signals before computing the temperature profile

The uncertainty components of the low and high channels due to detection noise are propagated to the merged signal profile assuming no correlation between the two channels:

$$u_{sM(SDET)}(k) = s_M(k)\sqrt{\left(w(k)\frac{u_{sm(DET)}(k,i_L)}{s_m(k,i_L)}\right)^2 + \left((1-w(k))\frac{u_{sm(DET)}(k,i_H)}{s_m(k,i_H)}\right)^2} \quad k_1 \le k \le k_2 \text{ and } 0 \le w(k) \le 1 \quad (66)$$

If the signal to be merged is the lidar-derived relative density ($s=N$), all uncertainty components due to atmospheric extinction propagate to the merge density using:

$$u_{sM(X)}(k) = s_M(k)\left(w(k)\frac{u_{sm(X)}(k,i_L)}{s_m(k,i_L)} + (1-w(k))\frac{u_{sm(X)}(k,i_H)}{s_m(k,i_H)}\right) \quad k_1 \le k \le k_2 \text{ and } 0 \le w(k) \le 1 \quad (67)$$

with $X = \sigma MR, \sigma MS, Na, \sigma igR, \sigma igS, Nig$.

For the uncertainty components of instrumental origin (namely, the saturation correction and background noise extraction), the degree of correlation between the channels hardware needs to be estimated before we can use a specific formulation for the propagation of the uncertainty components of instrumental origin. If the two channels use different hardware, they can be assumed independent and the merged signal uncertainties due to saturation correction and background noise extraction can be written

$$u_{sM(SX)}(k) = s_M(k)\sqrt{\left(w(k)\frac{u_{sm(X)}(k,i_L)}{s_m(k,i_L)}\right)^2 + \left((1-w(k))\frac{u_{sm(X)}(k,i_H)}{s_m(k,i_H)}\right)^2} \quad k_1 \le k \le k_2 \text{ and } 0 \le w(k) \le 1 \quad (68)$$

with $X = SAT, BKG$.

If the two channels share the same hardware and if the saturation and background noise corrections have been applied consistently for both channels within the same data processing algorithm, the associated uncertainty components can be propagated to the combined profile assuming full correlation:

$$u_{sM(X)}(k) = s_M(k)\left(w(k)\frac{u_{sm(X)}(k,i_L)}{s_m(k,i_L)} + (1-w(k))\frac{u_{sm(X)}(k,i_H)}{s_m(k,i_H)}\right) \quad k_1 \le k \le k_2 \text{ and } 0 \le w(k) \le 1 \quad (69)$$

with $X = SAT, BKG$.

The uncertainty components owing to temperature tie-on, acceleration of gravity, and the molecular mass of air are not included in the above expressions because they are introduced later in the data processing. In this case, the respective equations from sections 5.3.6 to 5.3.8 apply directly to the temperature profile retrieved from the merged lidar-derived number density.

5.4.2.2 Merging the temperature profiles retrieved for individual channels

The temperature uncertainty components of the low and high channels due to detection noise are propagated to the merged temperature profile assuming no correlation between the two channels:

$$u_{TM(DET)}(k) = \sqrt{\left(w(k)u_{Tm(DET)}(k,i_L)\right)^2 + \left((1-w(k))u_{Tm(DET)}(k,i_H)\right)^2} \quad k_1 \le k \le k_2 \text{ and } 0 \le w(k) \le 1 \quad (70)$$

For all uncertainty components that are not of instrumental origin, full correlation is assumed between the two channels:

$$u_{TM(X)}(k) = w(k)u_{Tm(X)}(k,i_L) + (1-w(k))u_{Tm(X)}(k,i_H) \quad \text{with } k_1 \le k \le k_2 \text{ and } 0 \le w(k) \le 1 \quad (71)$$

and $X = \sigma MR, \sigma MS, Na, \sigma igR, \sigma igS, Nig, g, TTOP, Ma$.

Just like in the case of merging the signals, for all uncertainty components of instrumental origin (namely, the saturation correction and background noise extraction) the degree of correlation between the channels hardware needs to be estimated. If the two channels use different hardware, they can be assumed independent and the temperature uncertainties due to saturation correction and background noise extraction can be written:

$$u_{TM(X)}(k) = \sqrt{\left(w(k)u_{Tm(X)}(k,i_L)\right)^2 + \left((1-w(k))u_{Tm(X)}(k,i_H)\right)^2} \quad k_1 \le k \le k_2 \text{ and } 0 \le w(k) \le 1 \qquad (72)$$

with $X = SAT, BKG$

If the two channels share the same hardware and if the saturation and background noise corrections have been applied consistently for both channels within the same data processing algorithm, the associated uncertainty components can be propagated to the combined profile assuming full correlation:

$$u_{TM(X)}(k) = w(k)u_{Tm(X)}(k,i_L) + (1-w(k))u_{Tm(X)}(k,i_H) \quad k_1 \le k \le k_2 \text{ and } 0 \le w(k) \le 1 \qquad (73)$$

with $X = SAT, BKG$.

Information / data	Type / value / equation	Notes / description
Name of effect	Merging of data from multiple channels	
Contribution identifier	4b	
Measurement equation parameter(s) subject to effect	P or T	Eq.9 or Eq.11
Contribution subject to effect (final product or sub-tree intermediate product)	T_M	Eq. 19
Time correlation extent & form	None	
Other (non-time) correlation extent & form	None	
Uncertainty PDF shape	N/A	
Uncertainty & units	Usually negligible	Depends on other corrections. For instance if uncertainty on the dead-time correction is large, the difference introduced in the merged profile is not negligible
Sensitivity coefficient	1	
Correlation(s) between affected parameters	Yes	1-3
Element/step common for all sites/users?	When multiple channels are available	
Traceable to ...	Leblanc et al., 2016d	
Validation	Jalali et al., 2016	

6 Uncertainty summary

Having reviewed and propagated all the independent uncertainty components considered in our lidar temperature measurement model, we can combine them into a unique temperature combined standard uncertainty:

$$u_T(k) = \sqrt{\begin{array}{l} u^2_{T(DET)}(k) + u^2_{T(SAT)}(k) + u^2_{T(BKG)}(k) + u^2_{T(TTOP)}(k) \\ + u^2_{T(\sigma MRand)}(k) + u^2_{T(\sigma MRSys)}(k) + u^2_{T(Na)}(k) + u^2_{T(g)}(k) + u^2_{T(Ma)}(k) \\ + u^2_{T(\sigma O3Rand)}(k) + u^2_{T(\sigma O3Sys)}(k) + u^2_{T(NO3)}(k) + u^2_{T(\sigma NO2Rand)}(k) + u^2_{T(\sigma NO2Sys)}(k) + u^2_{T(NNO2)}(k) \end{array}} \quad (74)$$

All uncertainty components should be set to zero at the tie-on altitude $z(k_{TOP})$, except for the uncertainty due to the ancillary temperature $u_{T(TTOP)}$. Also, when using multiple channels, the temperature combined standard uncertainty should not be computed for individual intensity channels and then merged into a single profile. Instead, the individual uncertainty components should first be propagated to the merged temperature profile and then added in quadrature to obtain the combined standard uncertainty.

When combining multiple profiles measured by the same instrument, for example to compute a climatology, uncertainty components due to systematic effects in altitude and/or time must remain separated from components due to random effects. Uncertainty due to detection noise is always added in quadrature, but for other components, knowledge of the covariance matrix in the time and/or altitude dimension(s) is required (type-A or type-B estimation).

Element identifier	Contribution name	Uncertainty contribution form	Typical value	Traceability level (L/M/H)	random, structured random, quasi-systematic or systematic?	Correlated to? (Use element identifier)
1	Alignment	N/A	negligible	M	Systematic	
2	**Pre-processing**					
2a	Detection noise	Poisson/ normal distribution	Large (>1 K) at the top of profile	H	random	
2b	Saturation correction	N/A	Large (~1 K) at low range of profile	H	systematic	
2c	Background noise correction	Poisson/ normal distribution	<0.3 K	H	random	
3	**External inputs**					
3a	Rayleigh extinction cross section	N/A	Large (~1 K) at low range of profile	H	Systematic	3b
3b	Air number density	N/A	Largest (<0.2 K) at low range of profile	M	Random and systematic	3a, 3f
3c1	Ozone cross section	N/A	up to 1 K error if neglected when working in the Chappuis band (e.g., 532	H	Random and systematic	3d1

			nm and 607 nm)			
3c2	NO_2 cross section	N/A	up to a 0.2 K error if neglected at 355 nm and 387 nm	H	systematic	3d2
3d1	Ozone profile	N/A	up to 1 K error if neglected when working in the Chappuis band (e.g., 532 nm and 607 nm)	M	Random and systematic	3c1
3d2	NO_2 profile	N/A	Depending on NO_2 density, but up to a 0.2 K error if neglected at 355 nm and 387 nm	L	Random and systematic	3c2
3e	Gravity	N/A	<0.2 K if altitude-/latitude-dependent gravity is used	H	systematic	
3f	Molecular mass of air	N/A	<0.1 K when altitude is below 90 km. Relevant when above 100 km.	H	systematic	
3g	External temperature at top	N/A	Large at top of profile	L/M	Random and systematic	
4	**Spatiotemporal integration**					
4a	Vertical filtering	N/A	Variable, Up to 2 K	H	systematic	
4b	Merging of multiple channels	N/A	Negligible	M	random	

An example uncertainty budget for the lidar at Mauna Loa is presented in Figure 8, where the individual contributions are given for the three channels covering the altitude domain and for the final merged product.

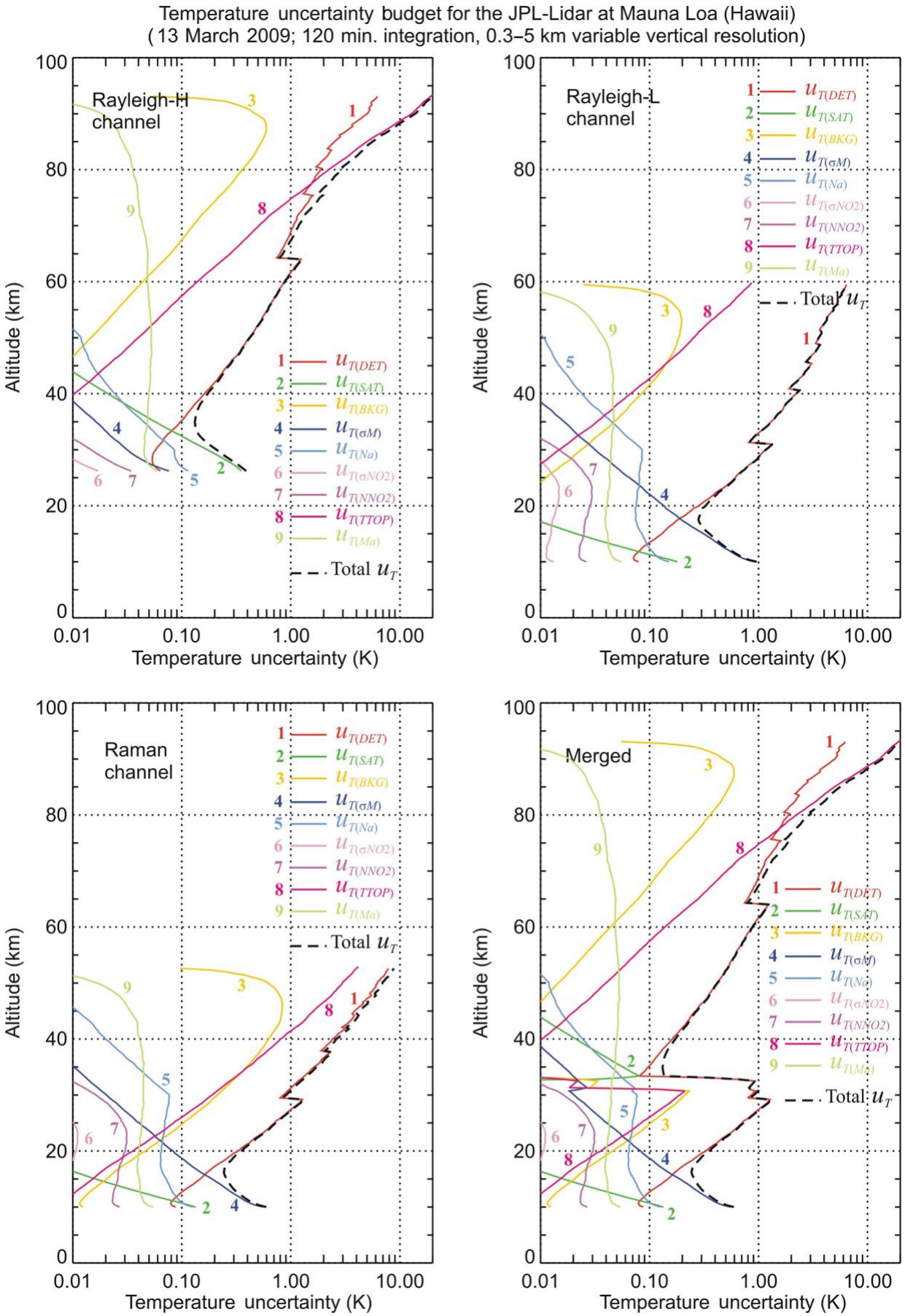

Figure 8. Example of uncertainty budget for the temperature retrievals done with the lidar at Mauna Loa for the high intensity Rayleigh channel (upper left), low intensity Rayleigh channel (upper right), the Raman channel (lower left) and the final profile combining these three channels. Figure reproduced from Leblanc et al., 2016c, their figure 10.

7 Traceability uncertainty analysis

The traceability level definition is given in Table 2.

Table 2. Traceability level definition table

Traceability Level	Descriptor	Multiplier
High	SI traceable or globally recognised community standard	1
Medium	Developmental community standard or peer-reviewed uncertainty assessment	3
Low	Approximate estimation	10

Analysis of the summary table would suggest the following contributions, shown in Table 3, should be considered further to improve the overall uncertainty of the NDACC temperature product. The entires are given in an estimated priority order.

Table 3. Traceability level definition further action table.

Element identifier	Contribution name	Uncertainty contribution form	Typical value	Traceability level (L/M/H)	random, structured random, quasi-systematic or systematic?	Correlated to? (Use element identifier)
3b	Profiles of number density or pressure and temperature	N/A	Largest (<0.2 K) at bottom of profile	M	Random and Systematic	3a
3d2	Profiles of interfering gases: NO_2	N/A	Depending on NO_2 density, but up to a 0.2 K error if neglected at 355 nm and 387 nm	L	Random and Systematic	3c
3g	External temperature at tie-on altitude	N/A	Large at top of profile, variable in value depending on closeness model/data	L/M	Random and Systematic	
4a	Vertical filtering	N/A	Variable, Up to 2 K	M	Random and Systematic	

7.1 Recommendations

It is recommended to further research the uncertainty sources that may be involved in the temperature profile retrievals with lidar. The two figures below provide an overview of identified (possible) sources/contributors of uncertainty for the instrumental part (Figure 9) and the processing software part (Figure 10).

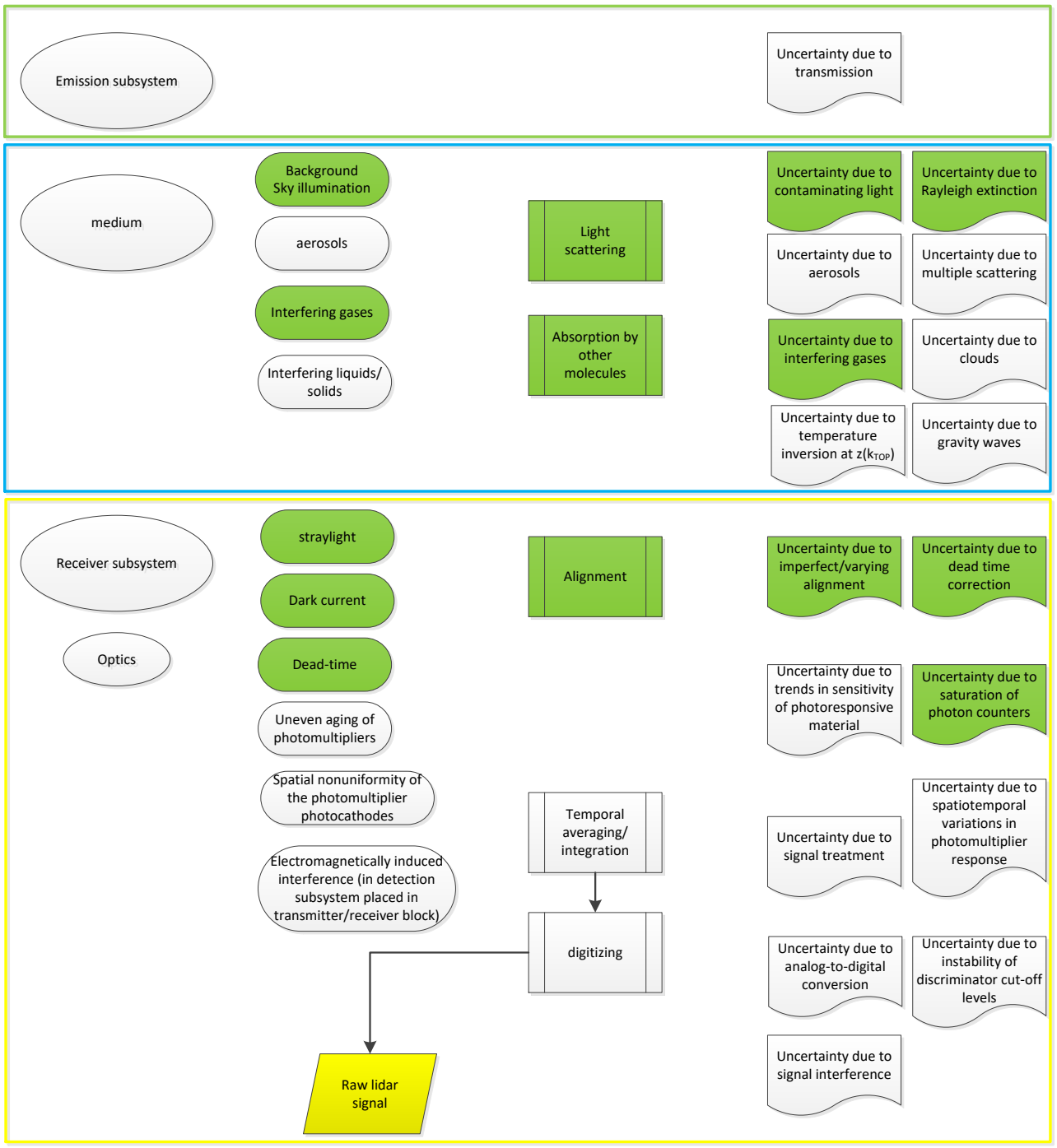

Figure 9. Additional possible sources of uncertainty in the instrumental part of the temperature profile retrieval. Green filled shapes have been discussed in this PTU, unfilled shapes have been identified as possible sources, but are considered negligible in many cases, highly variable, avoidable or complicated to determine.

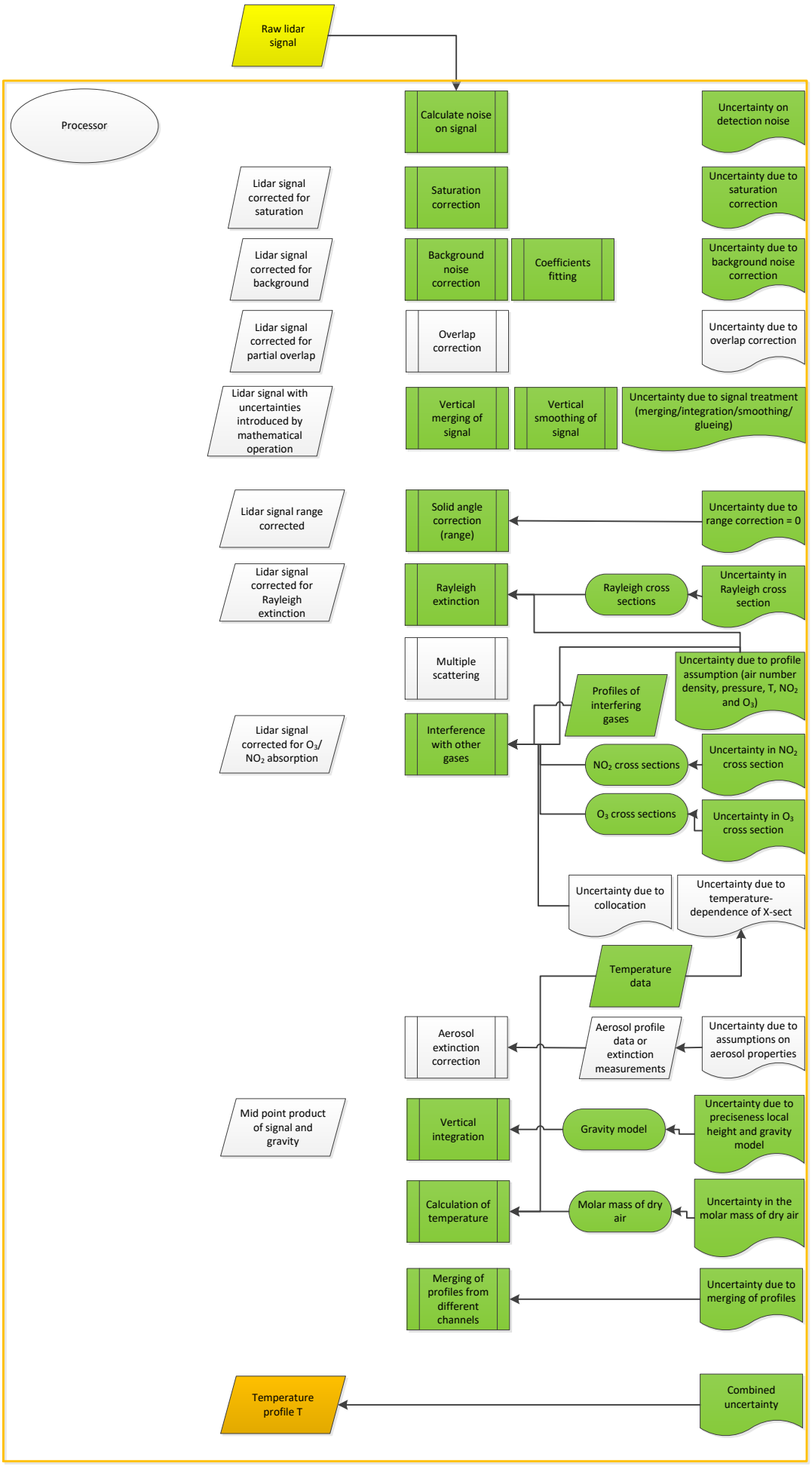
Raw lidar signal
Processor
Calculate noise on signal
Uncertainty on detection noise
Lidar signal corrected for saturation
Saturation correction
Uncertainty due to saturation correction
Lidar signal corrected for background
Background noise correction
Coefficients fitting
Uncertainty due to background noise correction
Lidar signal corrected for partial overlap
Overlap correction
Uncertainty due to overlap correction
Lidar signal with uncertainties introduced by mathematical operation
Vertical merging of signal
Vertical smoothing of signal
Uncertainty due to signal treatment (merging/integration/smoothing/ glueing)
Lidar signal range corrected
Solid angle correction (range)
Uncertainty due to range correction = 0
Lidar signal corrected for Rayleigh extinction
Rayleigh extinction
Rayleigh cross sections
Uncertainty in Rayleigh cross section
Multiple scattering
Uncertainty due to profile assumption (air number density, pressure, T, NO2 and O3)
Profiles of interfering gases
Lidar signal corrected for O3/ NO2 absorption
Interference with other gases
NO2 cross sections
Uncertainty in NO2 cross section
O3 cross sections
Uncertainty in O3 cross section
Uncertainty due to collocation
Uncertainty due to temperature-dependence of X-sect
Temperature data
Aerosol extinction correction
Aerosol profile data or extinction measurements
Uncertainty due to assumptions on aerosol properties
Mid point product of signal and gravity
Vertical integration
Gravity model
Uncertainty due to preciseness local height and gravity model
Calculation of temperature
Molar mass of dry air
Uncertainty in the molar mass of dry air
Merging of profiles from different channels
Uncertainty due to merging of profiles
Temperature profile T
Combined uncertainty

Figure 10. Continuation of Figure 9 with the processing software part.

8 Conclusion

The lidar temperature profile product has been assessed against the GAIA CLIM traceability and uncertainty criteria.

References

1. Ahmad, Z., McClain, C. R., Herman, J. R., Franz, B. A., Kwiatkowska, E. J., Robinson, W. D., Bucsela, E. J., and Tzortziou, M.: Atmospheric correction for NO_2 absorption in retrieving water-leaving reflectances from the SeaWiFS and MODIS measurements, Appl. Opt., 46(26), 6504-6512, 2007.
2. Argall, P. S.: Upper altitude limit for Rayleigh lidar, Ann. Geophys., 25, 19-25, 10.5194/angeo-25-19-2007, 2007.
3. Bates, D. R.: Rayleigh-scattering by air, Planet Space Sci., 32, 785-790, 10.1016/0032-0633(84)90102-8, 1984.
4. Bauer, R., Rozanov, A., McLinden, C. A., Gordley, L. L., Lotz, W., Russell, J. M., Walker, K. A., Zawodny, J. M., Ladstatter-Weissenmayer, A., Bovensmann, H., and Burrows, J. P.: Validation of SCIAMACHY limb NO_2 profiles using solar occultation measurements, Atmos. Meas. Tech., 5, 1059-1084, 10.5194/amt-5-1059-2012, 2012.
5. Bogumil, K., Orphal, J., Homann, T., Voigt, S., Spietz, P., Fleischmann, O. C., Vogel, A., Hartmann, M., Kromminga, H., Bovensmann, H., Frerick, J., and Burrows, J. P.: Measurements of molecular absorption spectra with the SCIAMACHY pre-flight model: instrument characterization and reference data for atmospheric remote-sensing in the 230-2380 nm region, J. Photochem. Photobiol. A, 157, 167-184, 10.1016/s1010-6030(03)00062-5, 2003.
6. Bracher, A., Sinnhuber, M., Rozanov, A., and Burrows, J. P.: Using a photochemical model for the validation of NO_2 satellite measurements at different solar zenith angles, Atmos. Chem. Phys., 5, 393-408, 10.5194/acp-5-393-2005, 2005.
7. Brion, J., Chakir, A., Charbonnier, J., Daumont, D., Parisse, C., and Malicet, J.: Absorption Spectra Measurements for the Ozone Molecule in the 350–830 nm Region, J. Atmos. Chem., 30, 291-299, 10.1023/a:1006036924364, 1998.
8. Bristow, M.P.: Lidar-signal compression by photomultiplier gain modulation: influence of detector nonlinearity, Appl. Opt. 37, 6468-6479, 1998.
9. Brohede, S., McLinden, C. A., Berthet, G., Haley, C. S., Murtagh, D., and Sioris, C. E.: A stratospheric NO_2 climatology from Odin/OSIRIS limb-scatter measurements, Can. J. Phys., 85, 1253-1274, 10.1139/p07-141, 2007.
10. Burkholder, J. B., and Talukdar, R. K.: Temperature dependence of the ozone absorption spectrum over the wavelength range 410 to 760 nm, Geophysical Research Letters, 21, 581-584, 10.1029/93gl02311, 1994.
11. Burrows, J. P., Richter, A., Dehn, A., Deters, B., Himmelmann, S., and Orphal, J.: Atmospheric remote-sensing reference data from GOME - 2. Temperature-dependent absorption cross-sections of O-3 in the 231-794 nm range, J. Quant. Spectr. Rad. Trans., 61, 509-517, 10.1016/s0022-4073(98)00037-5, 1999.
12. Chehade, W., Gorshelev, V., Serdyuchenko, A., Burrows, J. P., and Weber, M.: Revised temperature-dependent ozone absorption cross-section spectra (Bogumil et al.) measured with the SCIAMACHY satellite spectrometer, Atmos. Meas. Tech., 6, 3055-3065, doi:10.5194/amt-6-3055-2013, 2013.
13. Donovan, D. P., Whiteway, J. A., and Carswell, A. I.: Correction for nonlinear photon-counting effects in lidar systems, Appl. Opt., 32(33), 6742-6753, 1993.
14. Eberhard, W. L.: Correct equations and common approximations for calculating Rayleigh scatter in pure gases and mixtures and evaluation of differences, Appl. Opt., 49(7), 1116-1130, 2010.
15. Faduilhe, D., Keckhut P., Bencherif H., Robert L., Baldy S.: Stratospheric temperature monitoring using a vibrational Raman lidar. Part 1: Aerosols and ozone interferences, J. Environ. Monit., 7(4), 357-364, 2005.
16. Freudenthaler, V., Linné, H., Chaikovski, A., Rabus, D., and Groß, S.: EARLINET lidar quality assurance tools, Atmos. Meas. Tech. Discuss., doi:10.5194/amt-2017-395, in review,

2018.
17. Gorshelev, V., Serdyuchenko, A., Weber, M., Chehade, W., and Burrows, J. P.: High spectral resolution ozone absorption cross-sections - Part 1: Measurements, data analysis and comparison with previous measurements around 293 K, Atmos. Meas. Tech., 7, 609-624, 10.5194/amt-7-609-2014, 2014.
18. Gross, M. R., McGee, T. J., Ferrare, R. A., Singh, U. N., and Kimvilakani, P.: Temperature measurements made with a combined Rayleigh-Mie and Raman lidar, Appl. Opt., 36, 5987-5995, 1997.
19. Hauchecorne, A., and Chanin, M. L.: Density and temperature profiles obtained by lidar between 35-km and 70-km, Geophys. Res. Lett., 7, 565-568, 1980.
20. Hinkley, E. D.: Laser monitoring of the atmosphere, Topics in applied physics, 14, Springer-Verlag, New York, 380 pp., 1976.
21. Jalali, A, Sica, R.J. and Argall, P.S.: Extending and Merging the Purple Crow Lidar Temperature Climatologies Using the Inversion Method, ILRC27, EPJ Web of Conferences, 119, doi:10.1051/epjconf/201611917005, 2016.
22. Keckhut, P., Hauchecorne, A., and Chanin, M. L.: A critical-review of the database acquired for the long-term surveillance of the middle atmosphere by the French Rayleigh lidars, Journal of Atmospheric and Oceanic Technology, 10, 850-867, 10.1175/1520-0426(1993)010<0850:acrotd>2.0.co;2, 1993.
23. Keckhut, P., McDermid, S., Swart, D., McGee, T., Godin-Beekmann, S., Adriani, A., Barnes, J., Baray, J. L., Bencherif, H., Claude, H., di Sarra, A. G., Fiocco, G., Hansen, G., Hauchecorne, A., Leblanc, T., Lee, C. H., Pal, S., Megie, G., Nakane, H., Neuber, R., Steinbrecht, W., and Thayer, J.: Review of ozone and temperature lidar validations performed within the framework of the Network for the Detection of Stratospheric Change, J. Environ. Monit., 6, 721–733, doi:10.1039/b404256e, 2004.
24. Keckhut, P., Randel, W. J., Claud, C., Leblanc, T., Steinbrecht, W., Funatsu, B. M., Bencherif, H., McDermid, I. S., Hauchecorne, A., Long, C., Lin, R., and Baumgarten, G.: An evaluation of uncertainties in monitoring middle atmosphere temperatures with the ground-based lidar network in support of space observations, J. Atmos. Sol.-Terr. Phy., 73, 627–642, doi:10.1016/j.jastp.2011.01.003, 2011.
25. Leblanc, T., McDermid, I. S., Hauchecorne, A., and Keckhut, P.: Evaluation of optimization of lidar temperature analysis algorithms using simulated data, J. Geophys. Res., 103, 6177-6187, 1998.
26. Leblanc, T., Sica, R. J., van Gijsel, J. A. E., Godin-Beekmann, S., Haefele, A., Trickl, T., Payen, G., and Gabarrot, F.: Proposed standardized definitions for vertical resolution and uncertainty in the NDACC lidar ozone and temperature algorithms – Part 1: Vertical resolution, Atmos. Meas. Tech., 9, 4029-4049, https://doi.org/10.5194/amt-9-4029-2016, 2016a.
27. Leblanc, T., Sica, R. J., van Gijsel, J. A. E., Godin-Beekmann, S., Haefele, A., Trickl, T., Payen, G., and Liberti, G.: Proposed standardized definitions for vertical resolution and uncertainty in the NDACC lidar ozone and temperature algorithms – Part 2: Ozone DIAL uncertainty budget, Atmos. Meas. Tech., 9, 4051-4078, https://doi.org/10.5194/amt-9-4051-2016, 2016b.
28. Leblanc, T., Sica, R. J., van Gijsel, J. A. E., Haefele, A., Payen, G., and Liberti, G.: Proposed standardized definitions for vertical resolution and uncertainty in the NDACC lidar ozone and temperature algorithms – Part 3: Temperature uncertainty budget, Atmos. Meas. Tech., 9, 4079–4101, doi:10.5194/amt-9-4079-2016, 2016c.
29. Leblanc, T., Sica R., van Gijsel, J. A. E., Godin-Beekmann, S., Haefele, A., Trickl, T., Payen, G., and Liberti, G.: Standardized definition and reporting of vertical resolution and uncertainty in the NDACC lidar ozone and temperature algorithms, ISSI Team on NDACC Lidar Algorithms Report, available for download at: http://www.issibern.ch/teams/ndacc/ISSI_Team_Report.htm, 2016d.

30. Lemoine, F. C., Kenyon, S. C., Factor, J. K., Trimmer, R. G., Pavlis, N. K., Chinn, D. S., Cox, C. M., Klosko, S. M., Luthcke, S. B., Torrence, M. H., Wang, Y. M., Williamson, R. G., Pavlis, E. C., Rapp, R. H., and Olson, T. R.: The Development of the Joint NASA GSFC and the National Imagery and Mapping Agency (NIMA) Geopotential Model EGM96, Tech. Rep., 1998.
31. Mattis, I., D'Amico, G., Baars, H., Amodeo, A., Madonna, F., and Iarlori, M.: EARLINET Single Calculus Chain – technical – Part 2: Calculation of optical products, Atmos. Meas. Tech., 9, 3009–3029, doi:10.5194/amt-9-3009-2016, 2016.
32. Measures, R. M.: Laser remote sensing: fundamentals and applications, Wiley, 510 pp., 1984.
33. Mohr, P. J., Taylor, B. N., and Newell, D. B.: CODATA recommended values of the fundamental physical constants: 2006, Rev. Mod. Phys., 80, 633-730, 10.1103/RevModPhys.80.633, 2008.
34. Müller, J. W.: Dead-time problems, Nucl. Instr. and Meth., 112, 47-57, 10.1016/0029-554x(73)90773-8, 1973.
35. NIMA: Department of Defense World Geodetic System 1984, Tech. Rep., 3rd Edition, 175 pp available at: . earth-info.nga.mil/GandG/publications/tr8350.2/wgs84fin.pdf, 2000.
36. Press, W. H.; Flannery, B. P., Teukolsky, S. A., and Vetterling W. T.: Numerical Recipes: The Art of Scientific Computing (1st ed.), New York, Cambridge University Press. ISBN 978-0-521-88068-8, 1986.
37. She, C.Y., Alvarez, R.J., Caldwell, L.M. and Krueger, D.A.: High-spectral-resolution rayleigh-mie lidar measurement of vertical aerosol and atmospheric profiles, Appl. Phys. B, 55(22), 154-158, doi: 10.1007/BF00324067, 1992.
38. Sica, R. J., Zylawy, Z. A., and Argall, P. S.: Ozone Corrections for Rayleigh-Scatter Temperature Determinations in the Middle Atmosphere, J. Atmos. Ocean. Tech., 18, 1223-1228, doi:10.1175/1520-0426(2001)018<1223:OCFRST>2.0.CO;2, 2001.
39. Sica, R. J., and Haefele, A.: Retrieval of temperature from a multiple-channel Rayleigh-scatter lidar using an optimal estimation method, Appl. Opt., 54, 1872-1889, 10.1364/ao.54.001872, 2015.
40. Simeonov, V., Larcheveque, G., Quaglia, P., van den Bergh, H. and Calpini, V.: Influence of the photomultiplier tube spatial uniformity on lidar signals, Appl. Opt. 38, 5186-5190, 1999.
41. Strauch, R. G., Derr, V. E., and Cupp, R. E.: Atmospheric temperature measurement using raman backscatter, Appl. Opt., 10, 2665-&, 10.1364/ao.10.002665, 1971.
42. Strutt, J. W. (Lord Rayleigh): XXXIV. On the transmission of light through an atmosphere containing small particles in suspension, and on the origin of the blue of the sky, Philos. Mag., 47, 375-384, 10.1080/14786449908621276, 1899.
43. Vandaele, A. C., Hermans, C., Simon, P. C., Carleer, M., Colin, R., Fally, S., Merienne, M. F., Jenouvrier, A., and Coquart, B.: Measurements of the NO_2 absorption cross-section from 42 000 cm(-1) to 10 000 cm(-1) (238-1000 nm) at 220 K and 294 K, J. Quant. Spectr. Rad. Trans., 59, 171-184, 10.1016/s0022-4073(97)00168-4, 1998.
44. Weitkamp, C.: Lidar: Range-Resolved Optical Remote Sensing of the Atmosphere, Springer Series in Optical Sciences, 102, Springer, 460 pp., 2005.